Spring 5-13-2016

Poroacuatics Under Brinkman's Model

David A. Rossmanith Jr.
darossma@uno.edu

Poroacoustics Under Brinkman's Model

A Dissertation

Submitted to the Graduate Faculty of the
University of New Orleans
in partial fulfillment of the
requirements for the degree of

Doctor of Philosophy
in
Engineering and Applied Science
(Physics)

by

David Alan Rossmanith

B.S. University of New Orleans, 2008
M.S.A.P University of New Orleans, 2014

May, 2016

ACKNOWLEDGEMENTS

I would like to give thanks to Dr. Ashok Puri for his dedicated efforts as supervisor. He has guided me through the full path of research, from the beginnings of the idea, to the successful publication of several papers. His patience and guidance have been critical in my growth in this field.

I would also like to give special thanks to Dr. Pedro Jordan for his private communications and helpful insights. Dr. Jordan helped to introduce me into the field of poroacoustics, and has been kind enough to invite me to speak in his session at the 8th annual IMACS conference in Athens Georgia.

Finally, I would like to thank my family for their unending support. From the educational foundations and work ethic they instilled in me, to the patience and support they showed me during the long nights and weekends of research, I could not have gotten this far without being blessed with such an amazing family.

TABLE OF CONTENTS

LIST OF FIGURES

Figure

LIST OF TABLES

Table

ABSTRACT

Through perturbation analysis, a study of the role of Brinkman viscosity in the propagation of finite amplitude harmonic waves is carried out. Interplay between various parameters, namely, frequency, Reynolds number and beta are investigated. For systems with physically realizable Reynolds numbers, departure from the Darcy Jordan model (DJM) is noted for high frequency signals. Low and high frequency limiting cases are discussed, and the physical parameters defining the acoustic propagation are obtained.

Through numerical analyses, the roles of Brinkman viscosity, the Darcy coefficient, and the coefficient of nonlinearity on the evolution of finite amplitude harmonic waves is studied. An investigation of acoustic blow-ups is conducted, showing that an increase in the magnitude of the nonlinear term gives rise to blow-ups, while an increase in the strength of the Darcy and/or Brinkman terms mitigate them. Finally, an analytical study via a regular perturbation expansion is given to support the numerical results.

In order to gain insight into the formation and evolution of nonlinear standing waves under the Brinkman model, a numerical analysis is conducted on the weakly nonlinear model based on Brinkman's equation. We develop a finite difference scheme and conduct a parameter study. An examination of the Brinkman, Darcy, and nonlinear terms is carried out in the context of their roles on shock formation. Finally, we compare our findings to those of previous results found in similar nonlinear equations in other fields.

So as to better understand the behavior of finite-amplitude harmonic waves under a Brinkman-based poroacoustic model, approximations and transformations are used to recast the Brinkman equation into the damped Burger's equation. An examination is carried out

for the two special solutions of the damped Burger's equation: the approximate solution to the damped Burger's equation and the boundary value problem given an initial sinusoidal pulse. The effects of the Darcy coefficient, Reynolds number, and nonlinear coefficient on these solutions are investigated.

Keywords: Brinkman's equation; Poroacoustics; Nonlinear PDE; Perturbation; Finite difference

CHAPTER I

Introduction

1.1 Introduction

The science of fluid flow is a vast topic of great importance. Many different industries are interested in its study, including the medical field, oil exploration, hydrogeology, civil and environmental engineering, and continuum mechanics. This topic has been studied for quite some time and, while the fundamental theory is well understood, many problems arise when attempting to apply the theory to real world problems. Of major concern is the acoustic response of a viscous fluid saturating a porous medium.

Poroacoustics is the phenomenon in which an acoustic propagation in a viscous fluid is obtained within a porous medium *Jordan* (2009). This is of great use in the field of oil exploration, as studying the characteristics of sound signals sent through a porous sample could be used to identify the fluid which saturates the sample. Another example of the use of poroacoustics is in acoustic microscopy in the form of ultrasound testing. Sound propagation in buildings, building materials, and porous insulation is an example which is of great environmental concern. One very interesting use of acoustic waves in porous media is the drying of foodstuffs, such as apples. For more information on these, as well as other examples, see *Straughan* (2008) and the references found therein.

It is generally understood that Darcy's Law governs poroacoustic propagation *Nield and Bejan* (1999)

$$\nabla P = -\left(\frac{\mu\chi}{K}\right)\mathbf{V}, \tag{1.1}$$

where P is the intrinsic pressure, μ is the dynamic viscosity, χ is the porosity, K is the permeability, and $\mathbf{V}$ is the intrinsic velocity. This term (Darcy term), when applied as the acoustic potential, accounts for the fluid-pore interactions. However, it has been argued by Payne et al. *Payne et al.* (2001) that if a boundary or interface is present, or if the porosity is near unity, i.e. the fluid-pore interaction is not the dominating factor, then Brinkman's equation should be used *Nield and Bejan* (1999):

$$\nabla P = \tilde{\mu}\chi\nabla^2\mathbf{V} - \left(\frac{\mu\chi}{K}\right)\mathbf{V}. \tag{1.2}$$

Here, $\tilde{\mu}$ is the Brinkman or effective viscosity. This term accounts for the fluid-fluid interaction, as well as the fluid-pore interaction found in the Darcy term. It is the Brinkman equation which will be the focus of this paper.

In Chapter 2, we study (1.2) in the context of a semi-infinite medium with harmonic driving. We use perturbation analysis to investigate the role of the various terms in our equation. We then use a numerical scheme in Chapter 3 to investigate the evolution of a sinusoidal signal on a finite domain. We focus our analysis on blow-up formation and the mitigation of these blow-ups by the Darcy and Brinkman terms. Chapter 4 is an analysis of nonlinear standing waves with harmonic driving. Specifically, we investigate the sawtooth behavior which arises from the nonlinearity, and what roles the Brinkman and Darcy terms play in reducing this behavior. Chapter 5 is a study of (1.2) using known results from a similar equation (Burger's equation) in the context of traveling waves as well as the evolution of an initial sinusoidal signal. Finally, from these four analyses, we report our conclusions in Chapter 6.

CHAPTER II

Role of Brinkman Viscosity in Poroacoustic Propagation

2.1 Introduction

In order to gain a better understanding of the role that the Brinkman viscosity plays in the propagation of harmonic waves, we will carry out a perturbation analysis. With this analysis, we wish to study the interplay between the various physical parameters, such as Reynolds number, frequency, and β. We would like to discover any departure from the Darcy Jordan model (DJM), and for what range of frequencies this departure is found. Finally, we intend to derive the low and high frequency limits, and the the physical parameters that define the acoustic propagation.

2.2 Mathematical Formulation

Employing the methodology discussed in *Wei and Jordan* (2013), we obtain the basic governing equation for a weakly-nonlinear model based on (1.2). Assuming one-dimensional (1D) flow, conservation of mass takes the form

$$\rho_t + (\rho u)_x = 0, \tag{2.1}$$

where ρ is mass density and u is velocity. Here and henceforth, we will use the notation $\eta_i{:=}\partial\eta/\partial i$, where η is a general variable. The corresponding momentum equation is given by

$$\rho(u_t + uu_x) = -P_x + \tilde{\mu}\chi u_{xx} - \left(\frac{\mu\chi}{K}\right)u, \tag{2.2}$$

where P is the thermodynamic pressure and χ is the porosity. We now assume the quadratic approximation to the non-isentropic equation of state *Wei and Jordan* (2013),

$$P = P_e + \rho_e {c_e}^2[s + (\beta - 1)s^2 + \left(\frac{(\gamma - 1)}{\xi c_e^2}\right)(H - H_e)], \tag{2.3}$$

noting that the subscript e denotes the (constant) equilibrium state and c is the speed of sound in the undisturbed fluid, also referred to as the adiabatic sound speed, $\gamma = C_p/C_v$ is the adiabatic index, ξ is the thermal coefficient of volume expansion, and H is the specific entropy. Here β is the coefficient of non-linearity, $s = (\rho - \rho_e)/\rho_e$ is the condensation, and C_p and C_v denote the specific heats at constant pressure and volume respectively.

Finally, so that we can study the impact of Brinkman viscosity in isolation, we assume the flow to be homentropic, and thus the entropy production equation becomes

$$H = H_e. \tag{2.4}$$

This leads to the isentropic equation of state

$$P = P_e + \rho_e {c_e}^2[s + (\beta - 1)s^2]. \tag{2.5}$$

From these equations, eliminating P from (2.2) using (2.5) we get

$$\rho(u_t + uu_x) = -\rho_e {c_e}^2[s + (\beta - 1)s^2]_x + \tilde{\mu}\chi u_{xx} - \left(\frac{\mu\chi}{K}\right)u. \tag{2.6}$$

Next, noting that $u = \phi_x$, where $\phi = \phi\ (x,t)$ is the velocity potential, we introduce the

dimensionless quantities

$$\phi^o = \frac{\phi}{VL}, \quad u^o = \frac{u}{V}, \quad x^o = \frac{x}{L}, \quad t^o = \frac{tc_e}{L}. \tag{2.7}$$

Here, V and L are the characteristic speed and length, both positive, respectively. Also introducing the Mach number $\epsilon = V/c_e$, we then replace ρ with $\rho_e(1+s)$ in both (2.1) and (2.6). After further manipulation as well as using the binomial expansion approximation, dropping all terms of order $\mathcal{O}(\epsilon^2)$, we obtain *Jordan* (2009)

$$\Box^2\phi + \chi(Re)^{-1}\phi_{\mathrm{txx}} - \delta\phi_t = \epsilon\partial_t[(\beta-1)\phi_t^2 + \phi_x^2], \tag{2.8}$$

where $Re = c_e L\rho_e/\mu$, is a Reynolds number, $\delta \propto \chi$ is the dimensionless Darcy coefficient, and we have dropped the diamond superscripts on the dimensionless quantities.

2.3 Analytical Results

2.3.1 Perturbation Analysis

The perturbation approach used here closely follows that of *Jordan* (2009). We will start by stating the boundary-value problem (BVP)

$$\Box^2\phi + \chi(Re)^{-1}\phi_{\mathrm{txx}} - \delta\phi_t = \epsilon\partial_t[(\beta-1)\phi_t^2 + \phi_x^2], \tag{10}$$

$$\partial_x\phi(0,t) = \sin(\omega t), \tag{10a}$$

$$\partial_x\phi(\infty,t) = 0, \quad for(t>0), \tag{10b}$$

where $\Box^2 \equiv \partial_{\mathrm{xx}} - \partial_{\mathrm{tt}}$ is the 1D d'Alembertian operator. We will use ϵ as the perturbation parameter, noting however that because (10) was derived after dropping terms of order $\mathcal{O}(\epsilon^2)$, we can assume an expansion correct only to order $\mathcal{O}(\epsilon)$. Thus, with $\epsilon \mid \phi_1 \mid \ll \mid \phi_0 \mid$,

we set

$$\phi := \phi_0 + \epsilon\phi_1. \tag{2.9}$$

Substituting (2.9) into (2.10), and after expanding and equating like powers of ϵ, we get

$$\Box^2\phi_n + \chi(Re)^{-1}(\phi_n)_{\text{txx}} - \delta(\phi_n)_t = \begin{cases} 0, & n = 0, \\ [(\beta-1)(\phi_0)_t^2 + (\phi_0)_x^2]_t, & n = 1. \end{cases} \tag{2.10}$$

We now solve (2.10) subject to the boundary conditions:

$$(\phi_n)_x(0,t) = \begin{cases} \sin(\omega t), & n = 0, \\ 0, & n = 1, \end{cases} \qquad for\ \phi_{x_n}(\infty,t) = 0,\ n = 0,1. \tag{2.11}$$

Allowing $\phi_0(x,t) = \eta_0(x)\exp(-i\omega t) + c.c.$, where "$c.c.$" is the complex conjugate of the preceding term, the zeroeth order solution under the boundary conditions is determined to be

$$\phi_0(x,t) = \zeta_0 e^{-(\alpha_0 - i\beta_0)x} e^{-i\omega t} + c.c., \tag{2.12}$$

where $\zeta_0(\omega) = -(i/2)\left(\alpha_0 - i\beta_0\right)^{-1}$ and the corresponding attenuation coefficient and wavenumber are given, respectively, by

$$\begin{aligned} \alpha_0 &= \omega\sqrt{\frac{1 - Re^{-1}\delta\chi}{1 + Re^{-2}\chi^2\omega^2}}\sqrt{\frac{-1 + \sqrt{1 + \left(\frac{\delta\omega + Re^{-1}\chi\omega^3}{\omega^2 - Re^{-1}\delta\chi\omega^2}\right)^2}}{2}}, \\ \beta_0 &= \omega\sqrt{\frac{1 - Re^{-1}\delta\chi}{1 + Re^{-2}\chi^2\omega^2}}\sqrt{\frac{1 + \sqrt{1 + \left(\frac{\delta\omega + Re^{-1}\chi\omega^3}{\omega^2 - Re^{-1}\delta\chi\omega^2}\right)^2}}{2}}. \end{aligned} \tag{2.13}$$

Likewise, the first perturbation of ϕ_0 is determined by assuming a solution of the form $\phi_1(x,t) = \eta_1\exp(-2i\omega t) + c.c.$ and solving the inhomogeneous ODE (2.10)- (2.11) for n=1,

inserting ϕ_0 where appropriate. The solution takes the form

$$\phi_1(x,t) = [\zeta_1 e^{-(\alpha_1 - i\beta_1)x} + \psi_1 e^{-2(\alpha_0 - i\beta_0)x}]e^{-2i\omega t} + c.c., \tag{2.14}$$

$$\alpha_1 = 2\omega\sqrt{\frac{1 - Re^{-1}\delta\chi}{1 + 4Re^{-2}\chi^2\omega^2}}\sqrt{\frac{-1 + \sqrt{1 + \left(\frac{2\delta\omega + 8Re^{-1}\chi\omega^3}{4\omega^2 - 4Re^{-1}\delta\chi\omega^2}\right)^2}}{2}}, \tag{2.15}$$

$$\beta_1 = 2\omega\sqrt{\frac{1 - Re^{-1}\delta\chi}{1 + 4Re^{-2}\chi^2\omega^2}} * \sqrt{\frac{1 + \sqrt{1 + \left(\frac{2\delta\omega + 8Re^{-1}\chi\omega^3}{4\omega^2 - 4Re^{-1}\delta\chi\omega^2}\right)^2}}{2}},$$

with

$$\zeta_1 = \left(\frac{\omega((A_0)^2 - (-1+\beta)\omega^2)}{(A_0)(A_1)[-(A_1)^2 + 4(A_0)^2]}\right)\left(\frac{1}{(i + Re^{-1}\chi\omega)}\right),$$

$$\psi_1 = -\frac{1}{2}\frac{(\alpha_1 - i\beta_1)}{(\alpha_0 - i\beta_0)}\zeta_1.$$

For reasons of clarity, we have made the substitution $A_n = \alpha_n - i\beta_n$. Lastly, we substitute equations (2.12) and (2.14) into (2.9) to obtain the perturbed solution, allowing $U(x,t) = u_0 + \epsilon u_1$, where $u_0 \equiv (\phi_0)_x$and $u_1 \equiv (\phi_1)_x$.

2.3.2 Analysis

Figure 2.1 was plotted with low frequency and very high Reynolds number, of the order of 20,000. We have assumed the value of the nonlinearity coefficient $\beta = 3.625$. This corresponds to seawater at 20°C and 3.5% salinity *Beyer* (1997). With these values, we see a near perfect match to the DJM *Jordan* (2009).

Figure 2.2 is plotted with the same parameters as in Figure 2.1, but with varying values of the Reynolds number. It is quite easily seen that the velocity is sensitive to the Reynolds

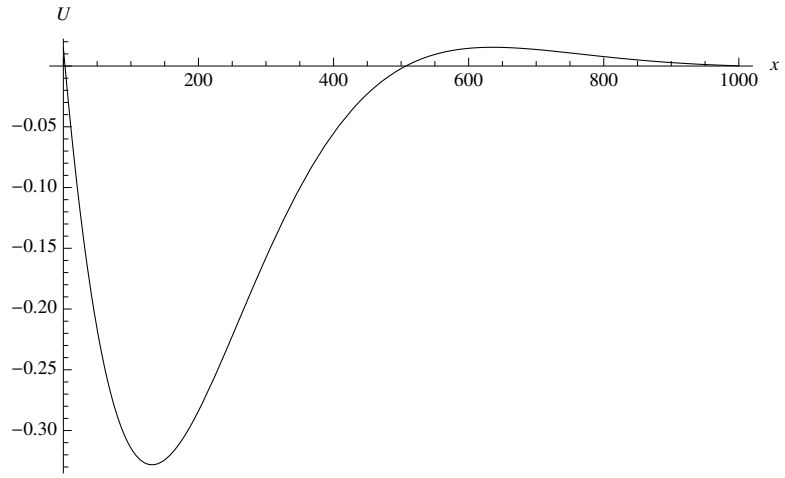

Figure 2.1: U vs x for $t = 10$, $\epsilon = 0.1$, $\delta = 0.05$, $\omega = 0.0015$, and Re = 20,000

number only for very low values of the Reynolds number which are, for the most part, unphysical. Figure 2.3, however, shows that for higher values of frequency, the Reynolds number in the physical regime becomes relatively more important.

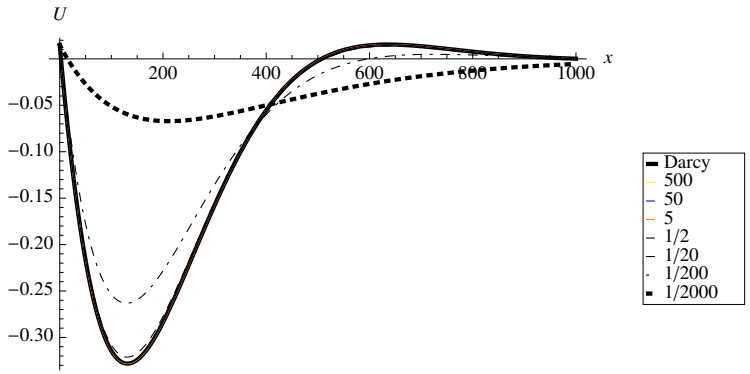

Figure 2.2: U vs x for $t = 10$, $\epsilon = 0.1$, $\delta = 0.05$, $\omega = 0.0015$, at varying Reynolds numbers

It is also of interest to note how different media respond to changes in Reynolds number. Figures 2.4 - 2.6 were plotted comparing different values of β for high frequency and low frequency respectively. Two disparate values of β were chosen for this comparison; $\beta = 4.4$, which corresponds to the liver *Wells* (1999), as well as $\beta = 1.077$ which corresponds to CO_2 at several thousand Kelvin *Thompson* (1972). It is quite evident from Figure 2.6 that β has little effect on the velocity in the low frequency regime, even over a wide range of Reynolds

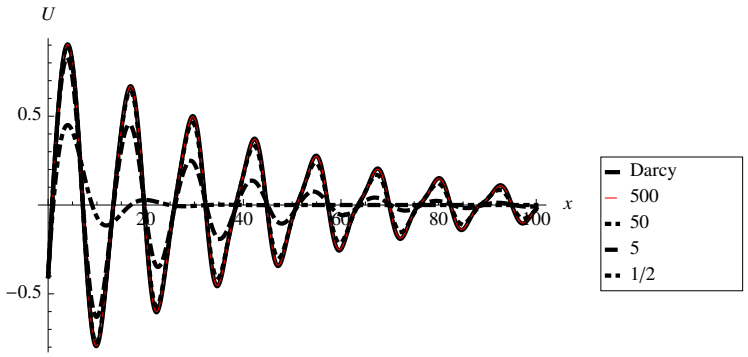

Figure 2.3: U vs x for $\beta = 3.625$, $t = 271$, $\epsilon = 0.01$, $\delta = 0.05$, $\omega = 0.5$, at varying Reynolds numbers

number. To show this more clearly, Figure 2.6(b) shows a plot of ϵu_1 vs x. There is only a slight distinction between the two β values. This difference is overwhelmed when the full solution is plotted. However, Figure 2.4 shows that for high frequencies, β does have a small impact for larger values of the Reynolds number.

To better show this effect, the first order correction term was plotted in Figures 2.5(a) and 2.5(b). It is clear why the impact of β is seen only for high Reynolds number systems. Because the β term is proportional to ω^3 through the time derivatives of the velocity potential, low frequency signals completely mute the β dependence. When high frequency signals are analyzed, the effect of the β term is realized for high Reynolds numbers. This is because the Brinkman term is linearly proportional to ω, through its single time derivative, and inversely proportional to the Reynolds number. Thus, in order to keep the Brinkman term from dominating the variations due to β, large values of the Reynolds number must be studied.

$\epsilon|u_1|$was plotted against x in Figure 2.7(a). We can see that it is bounded, going to zero with increasing x, and peaks much lower than unity. This helps ensure that the perturbation analysis is applicable, as the first order correction remains small compared to the zeroeth order term. To further show this, we plot the ratio of $\epsilon|u_1|$ to $|u_0|$ in Figure 2.7(b). It is clear from this figure that this ratio remains much less than unity for all values of the Reynolds

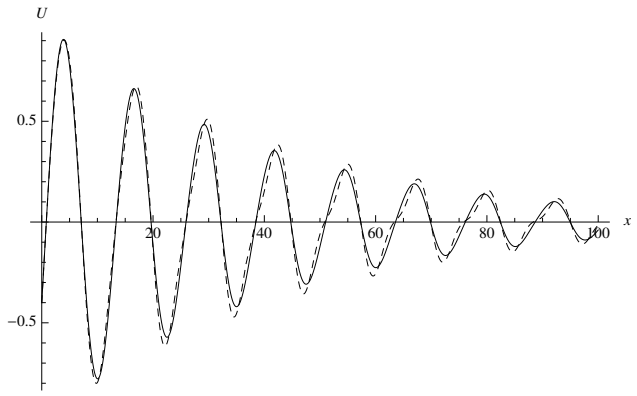

(a) High frequency, high Re.

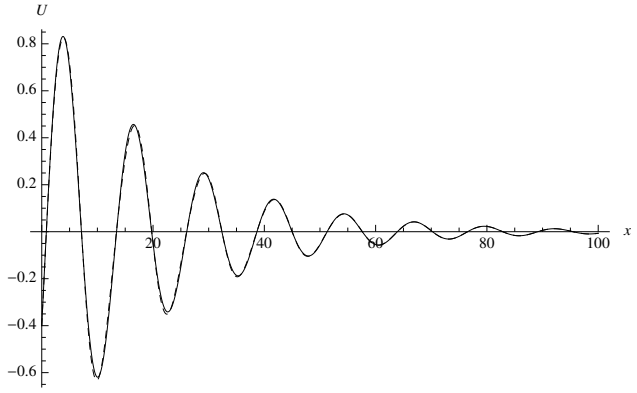

(b) High frequency, low Re.

Figure 2.4: U vs x for $t = 271$, $\epsilon = 0.01$, $\delta = 0.05$, $\omega = 0.5$. (a) $Re = 5{,}000$. (b) $Re = 5$. Solid: $\beta = 1.077$. Dashed: $\beta = 4.4$.

number.

Also of interest are the physical parameters defining the acoustic propagation, i.e. phase speed, penetration depth, and specific losses:

$$V_n = \frac{\omega}{\beta_n}, \quad d_n = \frac{1}{\alpha_n}, \quad \left(\frac{\Delta W}{W}\right)_n = 4\pi \left(\frac{\alpha_n}{\beta_n}\right) \quad (n = 0, 1). \tag{2.16}$$

More information about the physical significance of these parameters can be found in *Elmore and Heald* (1969); *Fetter and Walecka* (1980); *de Ville* (1996) respectively. We will derive low and high frequency approximations to the velocity potential as well as for the quantities

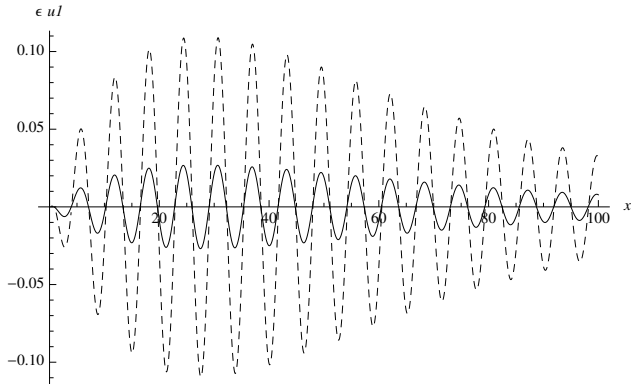

(a) High frequency, high Re.

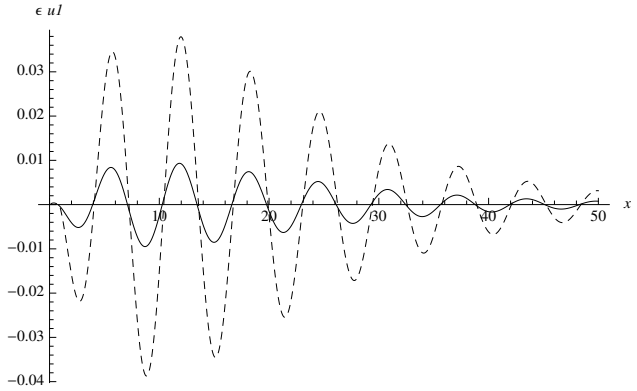

(b) High frequency, low Re.

Figure 2.5: ϵu_1 vs x for $t = 271$, $\epsilon = 0.01$, $\delta = 0.05$, $\omega = 0.5$. (a) $Re = 5{,}000$. (b) $Re = 5$. Solid: $\beta = 1.077$. Dashed: $\beta = 4.4$.

given in (2.16).

2.3.3 Low Frequency Approximation

From (2.13) and (2.3.1), we can rewrite $\alpha_{0,1}$ and $\beta_{0,1}$ in a more compact form:

$$\alpha_n = \omega(n+1)\xi_n \sqrt{\frac{-1+\sqrt{1+\left(\frac{\delta(\omega(n+1))\ +Re^{-1}\chi(\omega(n+1))^3}{(\omega(n+1))^2-Re^{-1}\delta\chi(\omega(n+1))^2}\right)^2}}{2}}, \tag{2.17}$$

$$\beta_n = \omega(n+1)\xi_n \sqrt{\frac{1+\sqrt{1+\left(\frac{\delta(\omega(n+1))\ +Re^{-1}\chi(\omega(n+1))^3}{(\omega(n+1))^2-Re^{-1}\delta\chi(\omega(n+1))^2}\right)^2}}{2}}.$$

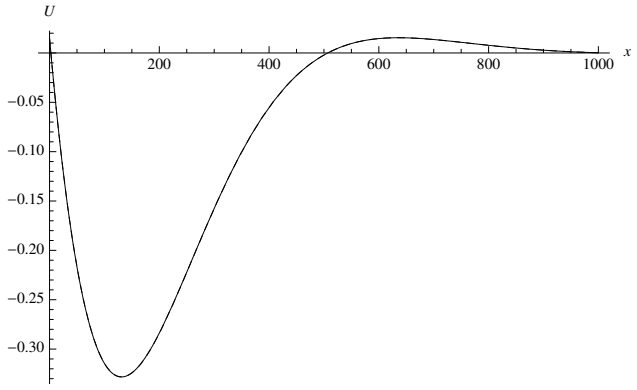

(a) Low frequency U vs x.

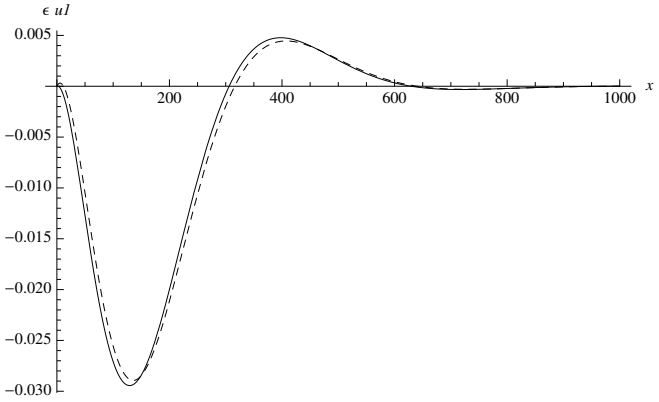

(b) Low frequency $\epsilon\ u_1$ vs x.

Figure 2.6: Solid: $\beta = 1.077$. Dashed: $\beta = 4.4$. (a) U vs x for $t = 10$, $\epsilon = 0.1$, $\delta = 0.05$, $\omega = 0.0015$, and $Re = 5{,}000$. (b) ϵu_1 vs x.

Supposing that $\omega \ll \delta$, then using the binomial expansion, α_n and $\beta_n$take on the form

$$\alpha_n \approx \frac{\omega(n+1)}{\sqrt{2}} \frac{\xi_n}{\gamma_n} \left(1 - \frac{{\gamma_n}^2}{2}\right),$$
$$\beta_n \approx \frac{\omega(n+1)}{\sqrt{2}} \frac{\xi_n}{\gamma_n} \left(1 + \frac{{\gamma_n}^2}{2}\right), \tag{2.18}$$

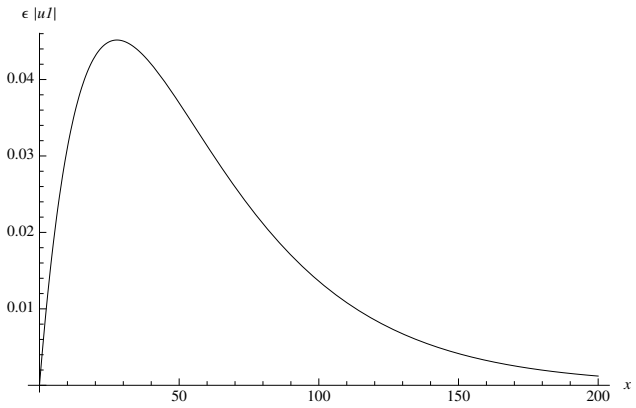

(a)

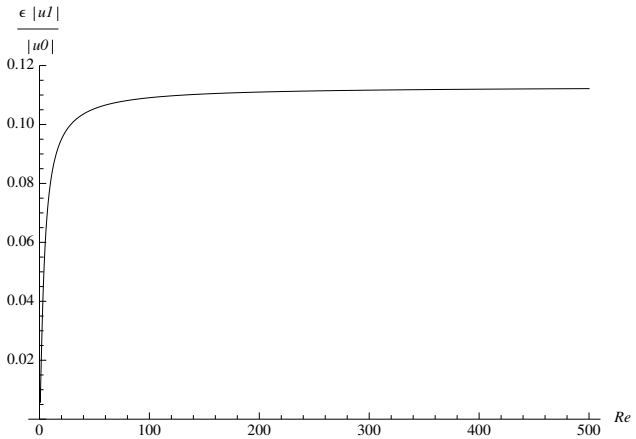

(b)

Figure 2.7:
(a) $\epsilon\ |u_1|$ vs x for $\epsilon = 0.01$, $\delta = 0.05$, $\beta = 3.625$
(b) $\epsilon\ |u1|\ /\ |u0|$ vs Re for $\epsilon = 0.01$, $\delta = 0.05$, $\beta = 3.625$

where

$$\xi_n = \sqrt{\frac{1 - Re^{-1}\delta\chi}{1 + Re^{-2}\chi^2(\omega(n+1))^2}},$$

$$\gamma_n = \left(\frac{1 - Re^{-1}\delta\chi}{\frac{\delta}{\omega(n+1)} + Re^{-1}\chi\omega} \right).$$

With these approximated values of the attenuation coefficient and wavenumber, we find that $U \approx u_{\mathrm{LF}}$. Figure 2.8 shows U vs x plotted with u_{LF} vs x for $\omega = .0015$. We find that

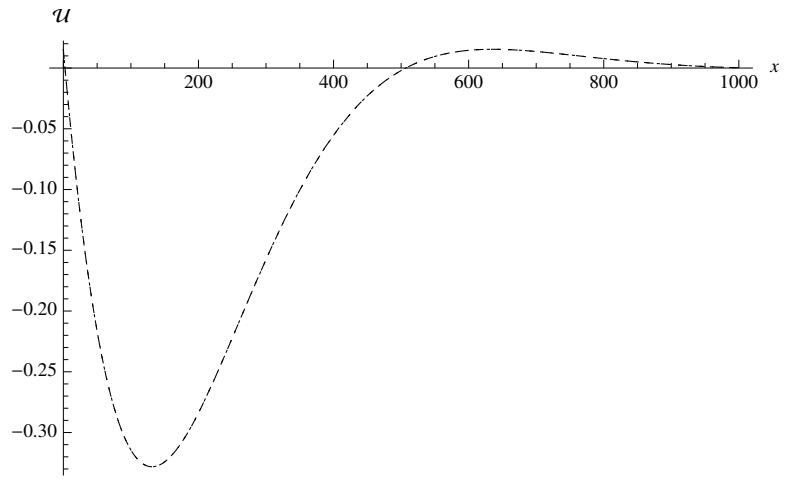

Figure 2.8: U vs x for $t = 10$, $\epsilon = 0.1$, $\delta = 0.05$, $\omega = 0.0015$, and Re = 20,000. Dashed: U. Dots: u_{LF}

the low frequency approximation is in excellent agreement with U. We can also give the low frequency approximations for the quantities in (2.16):

$$V_n = \frac{\omega}{\beta_n} \approx \gamma_n \frac{\sqrt{2}}{\xi_n}\left(1 - \frac{{\gamma_n}^2}{2}\right),$$
$$d_n = \frac{1}{\alpha_n} \approx \frac{\sqrt{2}}{\omega(n+1)}\frac{\gamma_n}{\xi_n}\left(1 + \frac{{\gamma_n}^2}{2}\right),$$
$$\left(\frac{\Delta W}{W}\right)_n = 4\pi\left(\frac{\alpha_n}{\beta_n}\right) \approx 4\pi\left(1 - \frac{{\gamma_n}^2}{2}\right) .$$

2.3.4 High Frequency Approximation

Now, under the assumption that $\omega \gg \delta$, we again use the binomial expansion to find the high frequency approximations of α_n and β_n:

$$\alpha_n \approx \frac{\xi_n \lambda_n^2}{2}\omega(n+1)\left(1 - \frac{1}{8}\lambda_n^2 + \frac{7}{128}\lambda_n^4\right), \tag{2.19}$$
$$\beta_n \approx \xi_n \omega(n+1)\left(1 + \frac{1}{8}\lambda_n^2 - \frac{5}{128}\lambda_n^4\right),$$

and the associated phase speed, penetration depth, and specific losses

$$V_n = \frac{\omega}{\beta_n} \approx \frac{1}{\xi_n(n+1)}\left(1 - \frac{{\lambda_n}^2}{8}\right),$$
$$d_n = \frac{1}{\alpha_n} \approx \frac{2}{\xi_n {\lambda_n}^2}\frac{1}{\omega(n+1)}\left(1 + \frac{{\lambda_n}^2}{8}\right),$$
$$\left(\frac{\Delta W}{W}\right)_n = 4\pi\left(\frac{\alpha_n}{\beta_n}\right) \approx 2\pi{\lambda_n}^2\left(1 - \frac{{\lambda_n}^2}{4}\right),$$

where

$$\lambda_n = \frac{\frac{\delta}{\omega(n+1)} + Re^{-1}\chi\omega(n+1)}{1 - Re^{-1}\delta\chi}.$$

Finally, we plot U vs. x along with its approximated high frequency solution u_{HF}, as shown in Figure 2.9. The high frequency approximation is in excellent agreement with U.

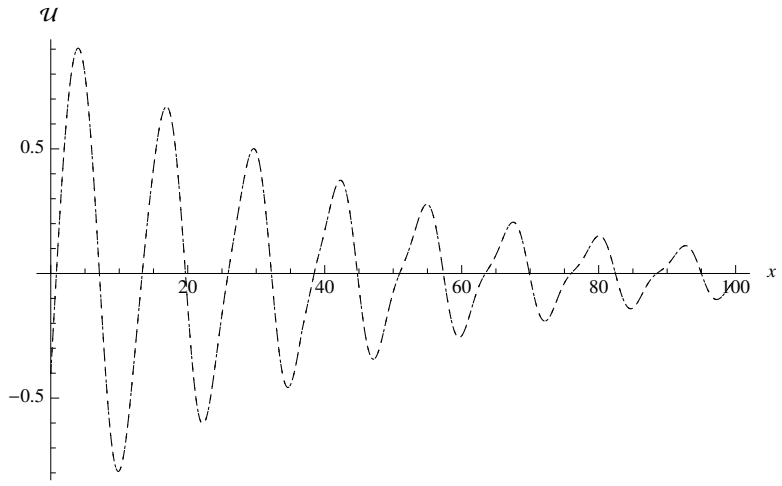

Figure 2.9: $\mathcal{U}$ vs x for $t = 271$, $\epsilon = 0.01$, $\delta = 0.05$, $\omega = 0.5$, and $Re = 20{,}000$. Dashed: U. Dots: u_{HF}

2.4 Discussion and Conclusion

In this chapter we have studied the behavior of the Brinkman equation under a time harmonic acoustic boundary condition. The problem was formulated using the governing conservation equations. A perturbation analysis was carried out, low and high frequency

limiting cases were discussed, and the physical parameters defining the acoustic propagation were obtained under those limiting cases. It is quite clear that the Reynolds number plays a role on the signal's ability to propagate. We have shown that for physically interesting systems (those with $Re \geq 5$), the Brinkman solution departs from the DJM only in the high frequency regime. Based on our analyses, we report the following :

1. The impact that the Brinkman viscosity term has on an acoustic signal, as can be seen in Figures 2.2 and 2.3, is found to be diffusive in nature, damping the signal faster than without its presence. With the Brinkman term being inversely proportional to the Reynolds number, high Reynolds number systems tend toward the Darcy Jordan model.

2. Because the Brinkman term is proportional to the acoustic frequency through the time derivative of the velocity potential, the diffusive effect is masked for lower frequencies, requiring a very low Reynolds number to reveal itself. However, for higher frequency signals, physically realistic Reynolds numbers, those of the order of 5 or more, give rise to a pronounced Brinkman viscosity dependence.

3. The coefficient of nonlinearity, β, can be interpreted as the term which describes the fluid through which the acoustic signal propagates. A β value of $1 \leq \beta \leq 1.35$ corresponds to perfect gases, while $\beta \geq 2.35$ corresponds to most liquids. As can be seen in Figures 2.4 and 2.5, the dependence on the coefficient of nonlinearity β is reduced by the Brinkman viscosity term. For high frequency signals, the dependence on β is only seen with very high Reynolds number systems, those with Reynolds numbers of 5,000 or more. Smaller Reynolds numbers increase the importance of the Brinkman term, masking the effects of changing β.

4. Figure 2.6 shows that there is little to no dependence on β for low frequency signals. This is due to the cubic dependence on ω through the time derivatives of the velocity potential in the nonlinear terms.

5. As can be seen from Figures 2.4 and 2.5, while a dependence on β is realized in the full solution, the dependence is most prevalent in the 1st order correction (nonlinear) term.

CHAPTER III

Nonlinear Evolution of a Sinusoidal Pulse Under a Brinkman-based Poroacoustic Model

3.1 Introduction

Through numerical analyses, we study the roles of Brinkman viscosity, the Darcy coefficient, and the coefficient of nonlinearity on the evolution of finite amplitude harmonic waves. An investigation of acoustic blow-ups is conducted, showing that an increase in the magnitude of the nonlinear term gives rise to blow-ups, while an increase in the strength of the Darcy and/or Brinkman terms mitigate them. Finally, an analytical study via a regular perturbation expansion is given to support the numerical results.

3.2 Mathematical Formulation and Problem Statement

As in *Rossmanith and Puri* (2014), we obtain the basic governing equation for a weakly-nonlinear model based on (1.2). Assuming 1D flow, conservation of mass, conservation of momentum, and the quadratic approximation to the isentropic equation of state *Wei and*

Jordan (2013) take the form:

$$\varrho_t + (\varrho u)_x = 0, \tag{3.1}$$

$$\varrho(u_t + uu_x) = -\mathcal{P}_x + \tilde{\mu}\chi u_{xx} - \left(\frac{\mu\chi}{K}\right) u, \tag{3.2}$$

$$\mathcal{P} = \mathcal{P}_e + \varrho_e {c_e}^2[s + (\beta - 1)s^2], \tag{3.3}$$

where ϱ is mass density and u is the velocity. Here and henceforth, we will use the notation $\eta_i{:=}\partial\eta/\partial i$, where η is a general variable. Note that the subscript e denotes the (constant) equilibrium state, c is the adiabatic speed of sound, β is the coefficient of nonlinearity, and $s = (\varrho - \varrho_e)/\varrho_e$ is the condensation.

From these equations, eliminating $\mathcal{P}$ from (3.2) using (3.3) we get,

$$\varrho(u_t + uu_x) = -\varrho_e {c_e}^2[s + (\beta - 1)s^2]_x + \tilde{\mu}\chi u_{xx} - \left(\frac{\mu\chi}{K}\right) u. \tag{3.4}$$

We now introduce the following dimensionless quantities, noting that $u = \phi_x$, where $\phi = \phi\,(x,t)$ is the velocity potential:

$$\begin{aligned} \phi^\diamond = \frac{\phi}{VL}, \quad u^\diamond = \frac{u}{V}, \quad x^\diamond = \frac{x}{L}, \\ t^\diamond = \frac{tc_e}{L}, \quad P^\diamond = \frac{\mathcal{P} - \mathcal{P}_e}{\varrho_e c_e V}. \end{aligned} \tag{3.5}$$

Here, V and L are the characteristic speed and length, both positive, respectively. Also, by introducing the Mach number $\epsilon = V/c_e$, and after further manipulation as well as using the binomial expansion approximation, dropping all terms of order $\mathcal{O}\,(\epsilon^2)$, we obtain *Jordan* (2009):

$$\Box^2\phi + \chi(Re)^{-1}\phi_{txx} - \delta\phi_t = \epsilon\partial_t[(\beta - 1)\phi_t^2 + \phi_x^2], \tag{3.6}$$

where $\Box^2 \equiv \partial_{xx} - \partial_{tt}$ is the 1D d'Alembertian operator, $Re = c_e L\sigma_e/\mu$, is a Reynolds number, $\delta \propto \chi$ is the dimensionless Darcy coefficient, and we have dropped the diamond

superscripts on the dimensionless quantities. As in *Crighton* (1979), we will now use the Lighthill-Westervelt approximation:

$$\phi_x \approx -\phi_t, \tag{3.7}$$

on the right hand side of (3.6). We next differentiate both sides of (3.6) with respect to t, and use the approximation:

$$P \approx -\phi_t, \tag{3.8}$$

which follows from (the dimensionless) Bernoulli's equation. This substitution, along with the following boundary and initial conditions, gives us the initial boundary-value problem (IBVP):

$$\Box^2 P + \chi(Re)^{-1} P_{txx} - \delta P_t = -2\epsilon\beta[(P_t)^2 + P(P_{tt})], \tag{3.9a}$$

$$P(x,0) = \sin(\pi x), \quad P_t(x,0) = 0, \quad for \quad (0 < x < 1) \tag{3.9b}$$

$$P(0,t) = 0, \quad P(1,t) = 0, \quad for \quad (t > 0). \tag{3.9c}$$

3.3 Numerical Analysis

3.3.1 Finite Difference Scheme Construction

With the IBVP having been stated, we will now make use of a finite difference scheme to find a numerical solution, meaning (3.9) must be discretized. The first step is to select the integers $I \geq 2$ and $J \geq 2$. Next, we set $\Delta x = T/I$ and $\Delta t = T/J$, where Δx and Δt denote uniform spatial and temporal step sizes, and T is the value of t for which the solution is sought. This gives the mesh points $x_i = i(\Delta x)$, for all $i = 0,1,...,I$, and $t_j = j(\Delta t)$, for all $j = 0,1,...,J$.

With this done, we will discretize (3.9a). We will start by replacing the second order derivatives with centered difference quotients, and first order derivatives with a backwards-Euler quotient. With these replacements, we obtain the difference equation,

$$\frac{P_{i+1}^j - 2P_i^j + P_{i-1}^j}{\Delta x^2} - \frac{P_i^{j+1} - 2P_i^j + P_i^{j-1}}{\Delta t^2} + \frac{\chi}{Re}\left[\frac{(P_{i+1}^j - 2P_i^j + P_{i-1}^j) - (P_{i+1}^{j-1} - 2P_i^{j-1} + P_{i-1}^{j-1})}{\Delta x^2 \Delta t}\right] - \delta\left(\frac{P_i^j - P_i^{j-1}}{\Delta t}\right) = -2\epsilon\beta\left[\left(\frac{P_i^j - P_i^{j-1}}{\Delta t}\right)^2 + P_i^j\left(\frac{P_i^{j+1} - 2P_i^j + P_i^{j-1}}{\Delta t^2}\right)\right], \tag{3.10}$$

where $P_i^j \approx P(x_i,t_j)$. Solving for the most advanced time step P_i^{j+1}, we obtain, after some manipulation, the explicit scheme:

$$P_i^{j+1} = \Delta t \frac{\chi}{Re}\left(\frac{P_{i-1}^{j-1} - P_{i-1}^j - 2P_i^{j-1} + 2P_i^j + P_{i+1}^{j-1} - P_{i+1}^j}{\Delta x^2(2\epsilon\beta P_i^j - 1)}\right) + \Delta t^2\left(\frac{-P_{i-1}^j + 2P_i^j - P_{i+1}^j}{\Delta x^2(2\epsilon\beta P_i^j - 1)}\right) + \Delta t\delta\left(\frac{-P_i^{j-1} + P_i^j}{2\epsilon\beta P_i^j - 1}\right) + \left(\frac{P_i^{j-1} - 2\delta P_i^j + 2\epsilon\beta((P_i^j)^2 + P_i^{j-1}P_i^j - (P_i^{j-1})^2)}{2\epsilon\beta P_i^j - 1}\right). \tag{3.11}$$

The last step involves discretizing the initial and boundary conditions (3.9b) and (3.9c). For details on this straightforward process see *Burden and Faires* (1993). The resulting conditions are as follows:

$$P_i^0 = \sin(\pi x_i), \tag{3.12a}$$

$$\partial_t P_i^0 = 0, \tag{3.12b}$$

$$P_0^j = 0, \tag{3.12c}$$

$$P_I^j = 0. \tag{3.12d}$$

3.3.2 Numerical Results

Figure 3.1 is a plot of the pressure, P, as a function of position, versus time. It was plotted with high Darcy coefficient and very high Reynolds number, of the order of 20,000. We have assumed a mach number of .01 and a value of the nonlinearity coefficient $\beta = 3.625$. This corresponds to seawater at 20°C and 3.5% salinity *Beyer* (1997). These values would diminish the Brinkman term enough to force the system to correspond to the Darcy-Jordan Model (DJM) *Jordan* (2009). We see that the system does indeed evolve like a damped oscillator.

Figure 3.2 shows the corresponding amplitude of the pressure as a function of position at

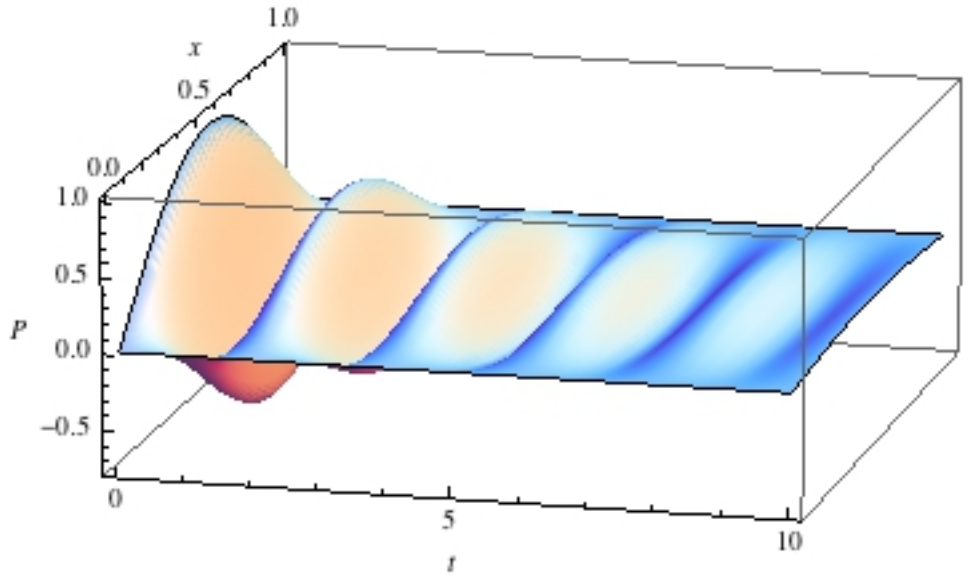

Figure 3.1: P vs x vs t for $\epsilon = 0.01$, $\delta = 0.5$, $\chi = .9$, $\beta = 3.625$, and $Re = 20{,}000$

various time snapshots.

3.4 Parameter Study

In order to further understand (3.9a), we carry out a parameter study, analyzing each term in the equation to learn of their relevance.

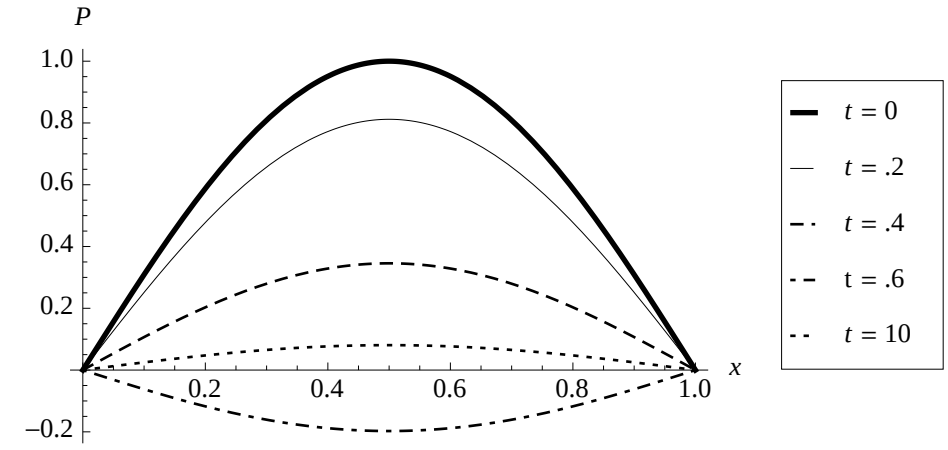

Figure 3.2: P vs x for $\epsilon = 0.01$, $\delta = 0.5$, $\chi = 0.9$, $\beta = 3.625$, and $Re = 20{,}000$ at varying times

3.4.1 Darcy Term

Our first study is that of the Darcy term. Setting Re to infinity and ϵ to zero in (3.9a) allows us to plot Figure 3.3. Here, we see that the Darcy term acts to dampen the signal. Increasing δ from a relatively low value of 0.15 to a large value of 0.5 increases the strength of the Darcy term, giving rise to a very fast decay of the signal.

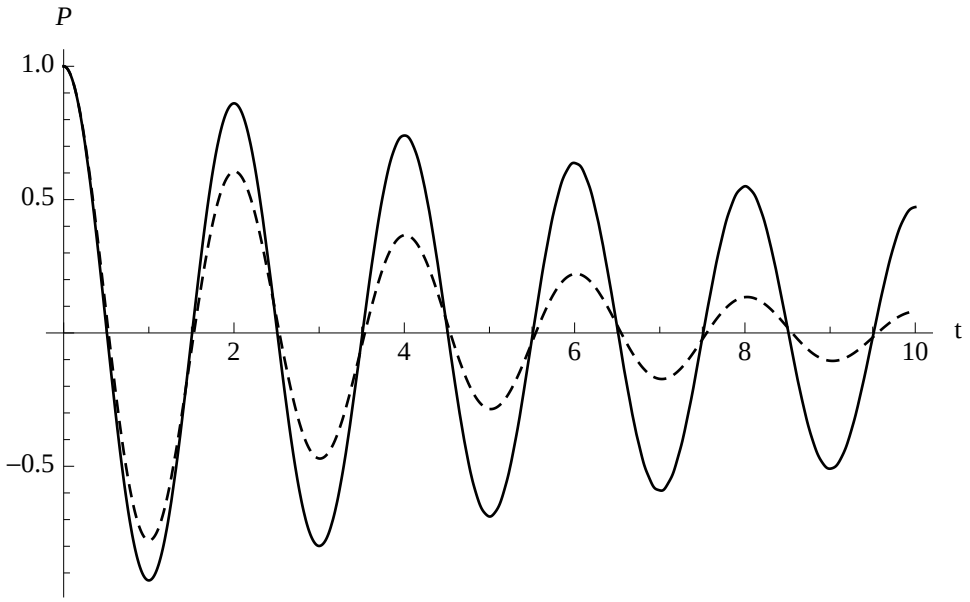

Figure 3.3: P vs t for $x = 0.5$. Solid: $\delta = 0.15$. Dashed: $\delta = 0.5$.

3.4.2 Brinkman Term

We will use a similar technique to study the role of the Brinkman term, by setting δ and ϵ to zero in (3.9a). The results are plotted in Figure 3.4. When the Brinkman term is strong, the solution is diffusive, as seen in the solid curve. However, as Re is increased, the Brinkman term is weakened, and the solution shifts towards a damped oscillatory behavior, as in the Darcy case.

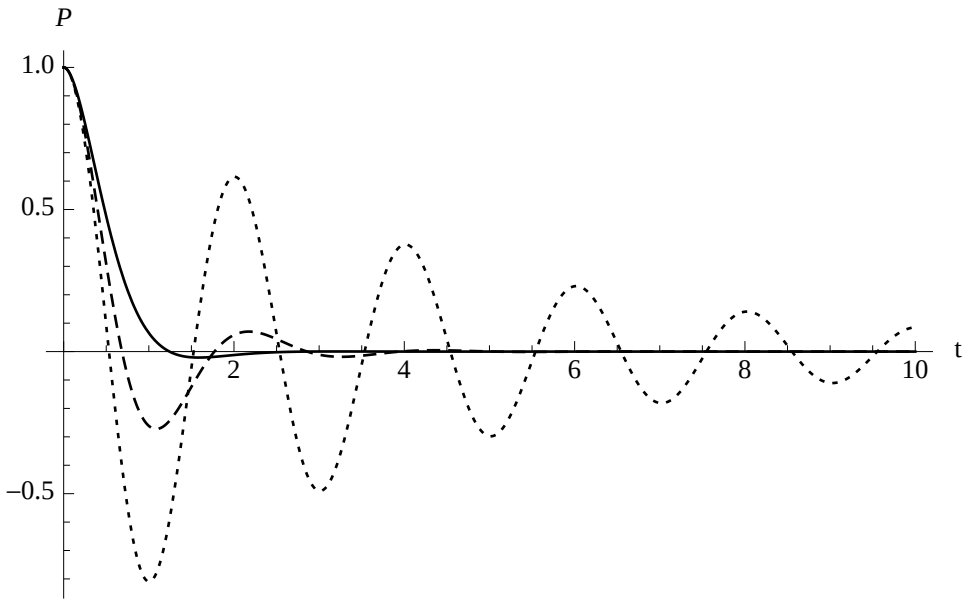

Figure 3.4: P vs t at $x = 0.5$, for $\chi = 0.9$. Solid: $Re = 2$. Dashed: $Re = 4$. Dotted: $Re = 20$.

3.4.3 Nonlinearity

We next study the nonlinear term, in particular its role in causing a finite time blow-up. It has been shown in *Jordan* (2004) and *Jordan* (2009) that equations similar to the present study give rise to similar blow-ups. First we will see the nonlinear terms' effects without the Brinkman term in Figure 3.5.

Figure 3.5 shows a plot of the pressure as a function of position vs time, as well as a plot of various time snapshots of the pressure vs position, for different values of the product $\epsilon\beta$. Figures 3.5(a) and 3.5(b) are plotted with $\delta = 0.005$, a moderate mach number, $\epsilon = .1$, as

well as $\beta = 3.625$. We see that the inclusion of a moderate nonlinearity gives rise to a blow up occurring at $t \sim 7.63$. Figure 3.5(b) in particular shows the beginning of the blow-up, with the $t = 7.63$ curve showing a maximum amplitude dipping below -1. Since the initial amplitude was $P = 1$, this is obviously forbidden, and thus a clear sign of a blow-up. We then continue to increase β to 4.0 in Figures 3.5(c) and 3.5(d). We now see that the blow-up occurs at a much earlier time, $t \sim 5.65$.

To see how the Darcy term could effect the system's ability to form a blow-up, we increase the value of δ from .005 to .05 in Figures 3.5(e) and 3.5(f). We see that the blow-up does not occur at $t = 5.65$ anymore. In fact, the blow-up does not occur at all during the full period of study. This is expected from the results of Figure 3.3. It appears that the Darcy term acted to dampen the signal sufficiently quickly to prevent the blow-up from occurring.

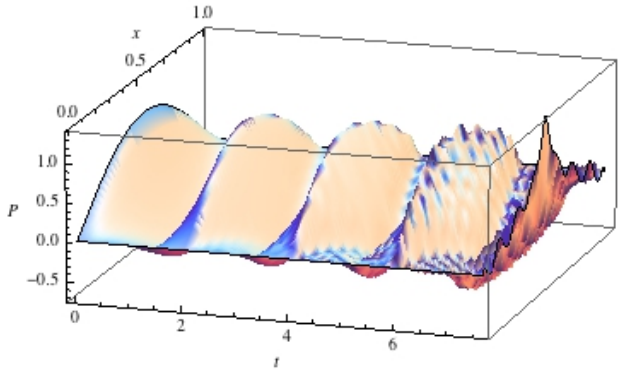

(a) P vs x vs t.

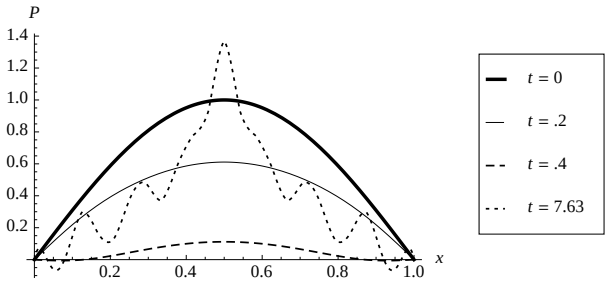

(b) P vs x.

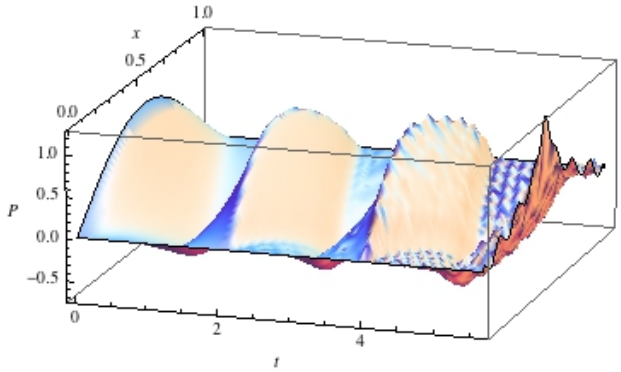

(c) P vs x vs t.

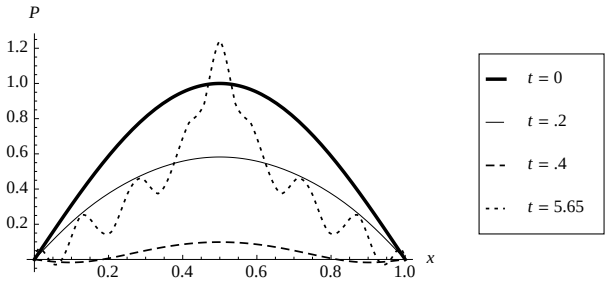

(d) P vs x.

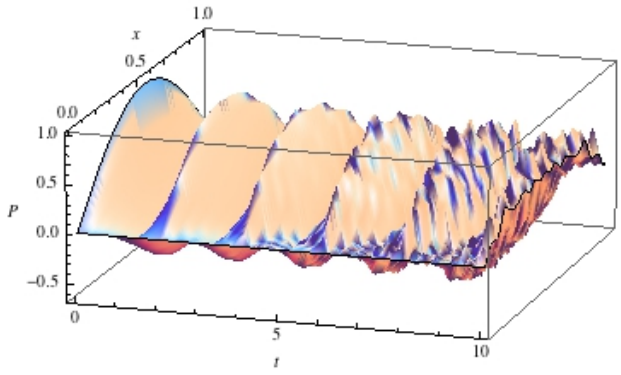

(e) P vs x vs t.

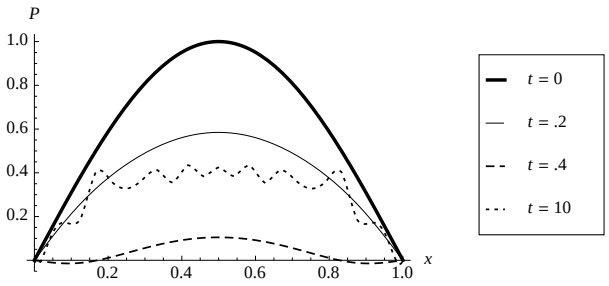

(f) P vs x.

Figure 3.5: (a)&(b) $\epsilon = .1$, $\beta = 3.625$, and $\delta = .005$. (c)&(d) $\epsilon = 0.1$, $\beta = 4.0$, and $\delta = .005$. (e)&(f) $\epsilon = 0.1$, $\beta = 4.0$, and $\delta = .05$.

	$\delta = 0.01$	$\delta = 0.025$	$\delta = 0.05$
$\epsilon\beta = 0.30$	$t > 10$	$t > 10$	$t > 10$
$\epsilon\beta = 0.3625$	$t = 9.59$	$t > 10$	$t > 10$
$\epsilon\beta = 0.38$	$t = 7.61$	$t = 9.67$	$t > 10$
$\epsilon\beta = 0.40$	$t = 5.67$	$t = 7.62$	$t > 10$
$\epsilon\beta = 0.45$	$t = 3.69$	$t = 5.61$	$t = 5.66$

Table 3.1: Blow-up time as a function of δ and $\epsilon\beta$.

Table 3.1 shows the relationship between blow-up time, $\epsilon\beta$, and δ. We see that as $\epsilon\beta$ is increased, the blow-up time is reduced. We also see that the blow up time is quite sensitive to δ. As δ is increased, the blow-up time is shifted to later times.

We now study the effects of the nonlinear term in conjunction with the Brinkman term, in two regimes. The Brinkman term, while in its diffusive regime (low Re) does not allow for the formation of blow-ups, as seen in Figure 3.5. Increasing $\epsilon\beta$ to values as high as 0.4 has very little effect on the signal due to its diffusive nature in this regime.

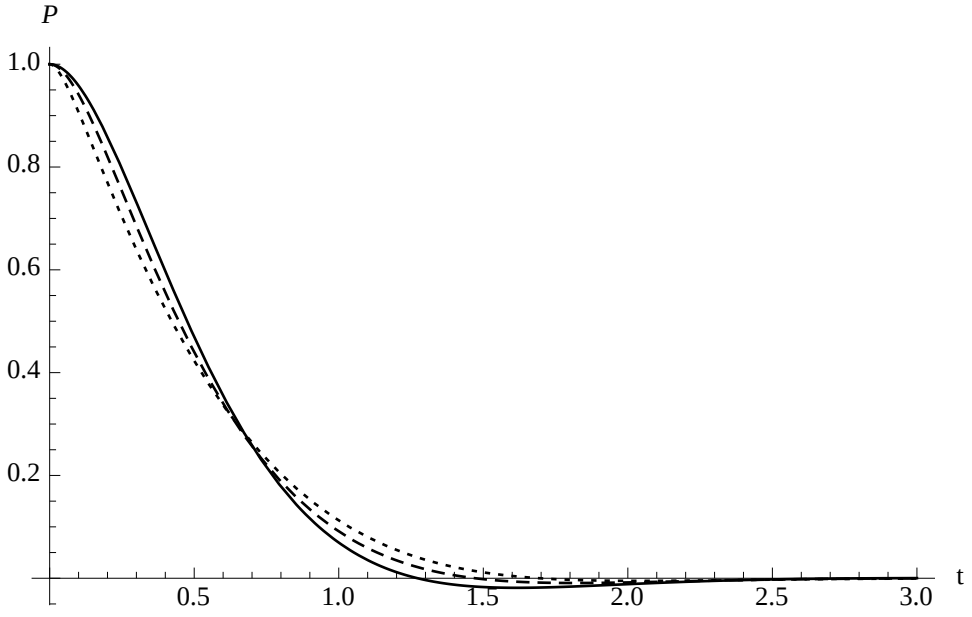

Figure 3.6: P vs t at $x = 0.5$, for $\chi = 0.9$ and $Re = 2$. Solid: $\epsilon\beta = 0$. Dashed: $\epsilon\beta = 0.2$. Dotted: $\epsilon\beta = 0.4$.

However, blow-ups do become an important factor when we consider the Brinkman term in the hyperbolic (high Re) regime. Table 3.2 shows the interplay between Re, $\epsilon\beta$, and blow-up times. We see that setting a moderate value of $\epsilon\beta$, of the order of 0.35, allows for the formation of blow-ups. Increasing the value of $\epsilon\beta$ shifts the blow-ups to earlier times. We also see from Table 3.2 that, for fixed $\epsilon\beta$, as Re is decreased, the Brinkman term is strengthened and the blow-ups are mitigated, similar to the behavior noted with the Darcy term.

	$Re = 10{,}000$	$Re = 2{,}000$	$Re = 1{,}000$
$\epsilon\beta = 0.30$	$t > 10$	$t > 10$	$t > 10$
$\epsilon\beta = 0.35$	$t = 9.58$	$t > 10$	$t > 10$
$\epsilon\beta = 0.3625$	$t = 7.62$	$t > 10$	$t > 10$
$\epsilon\beta = 0.38$	$t = 5.67$	$t = 9.56$	$t > 10$
$\epsilon\beta = 0.40$	$t = 5.65$	$t = 7.59$	$t > 10$
$\epsilon\beta = 0.45$	$t = 3.61$	$t = 3.7$	$t = 5.62$

Table 3.2: Blow-up time as a function of Re and $\epsilon\beta$.

3.5 Analytical Results

3.5.1 Perturbation Analysis

In order to help verify our numerical work, we will now give an analytical study of (3.9a). We will use a perturbation approach which closely follows that discussed in *Rossmanith and Puri* (2014) and *Jordan* (2009). Using ϵ as the perturbation parameter, we note that because (3.7) was derived after dropping terms of order $\mathcal{O}(\epsilon^2)$, we can assume an expansion correct only to order $\mathcal{O}(\epsilon)$. Thus, with $\epsilon |P_1| \ll |P_0|$, we set

$$P := P_0 + \epsilon P_1. \tag{3.13}$$

Substituting (3.13) into (3.9), and after expanding and equating like powers of ϵ, we get:

$$\Box^2 P_i + \chi(Re)^{-1}(P_i)_{txx} - \delta(P_i)_t = \begin{cases} 0, & i = 0, \\ -2\epsilon\beta[(\partial_t P_0)^2 + P_0(\partial_{tt} P_0)], & i = 1. \end{cases} \tag{3.14}$$

We will make use of finite sine transforms as well as Laplace transforms to solve (3.14). Let $\mathcal{S}(f(t,x))$ and $\mathcal{L}(f(t,x))$ denote the finite sine transform and Laplace transform of $f(t,x)$ respectively. Then,

$$\mathcal{S}(P_0[t,x]) = \psi_0[t,n], \tag{3.15a}$$

$$\mathcal{S}(\partial_t P_0[t,x]) = \partial_t \psi_0[t,n], \tag{3.15b}$$

$$\mathcal{S}(\partial_{xx} P_0[t,x]) = -\left(\frac{n\pi}{L}\right)^2 \psi_0[t,n] + \frac{2n\pi}{L^2}\left(P_0[t,0] + (-1)^{n+1} P_0[t,L]\right), \tag{3.15c}$$

$$\mathcal{S}(\partial_{txx} P_0[t,x]) = -\left(\frac{n\pi}{L}\right)^2 \partial_t \psi_0[t,n] + \frac{2n\pi}{L^2}\left(\partial_t P_0[t,0] + (-1)^{n+1} \partial_t P_0[t,L]\right), \tag{3.15d}$$

and,

$$\mathcal{L}(\psi_0[t,n]) = \zeta_0[s,n], \tag{3.16a}$$

$$\mathcal{L}(\partial_t \psi_0[t,n]) = s\zeta_0[s,n] - \psi[0,n], \tag{3.16b}$$

$$\mathcal{L}(\partial_{tt} \psi_0[t,n]) = s^2\zeta_0[s,n] - s\psi[0,n] - \partial_t \psi[0,n]. \tag{3.16c}$$

Applying (3.15) to (3.14), we get for zeroth order:

$$-\left(\frac{n\pi}{L}\right)^2 \psi_0[t,n] - \partial_{tt}\psi_0[t,n] - \left(\frac{n\pi}{L}\right)^2 \partial_t \psi_0[t,n] - \delta\partial_t \psi_0[t,n] = 0 \tag{3.17}$$

Next we will apply the Laplace transform to (3.17), use the initial and boundary conditions, and solve for ζ_0 to get:

$$\zeta_0[s,n] = \frac{s + \delta + \pi^2 \frac{\chi}{Re}}{s\,(s+\delta) + \pi^2\left(1 + s\frac{\chi}{Re}\right)}. \tag{3.18}$$

Taking the inverse Laplace transform and inverse sine transform yields:

$$P_0 = e^{\frac{t}{2}\mu} \sin(\pi x) \frac{\left(\xi \cosh\left(\frac{t}{2}\xi\right) + \mu \sinh\left(\frac{t}{2}\xi\right)\right)}{\xi}, \tag{3.19}$$

where,

$$\xi = \sqrt{\tau^2 - 4\pi^2}, \tag{3.20a}$$

$$\tau = \delta + \pi^2 \frac{\chi}{Re}. \tag{3.20b}$$

This result matches the exact analytical result found in *R.E. Mickens* (2004) for the damped wave equation by setting the Brinkman coefficient $\chi/Re = 0$ in Equations (3.19)-(3.20).

We next follow this same procedure for the first order correction term. Plugging in the resulting solution, along with (3.19), into (3.13), we plot Figure 3.7. There is a near perfect match with the numerical results. Figure 3.8 plots ϵP_1 vs x, further comparing the numerical work to the perturbation analysis. Again, we see an excellent match between the numerical and perturbation results. Of course, because this perturbation approach used ϵ as the perturbation parameter, this analysis only holds true for small nonlinearities. Thus it can not be used to study blow-ups.

3.6 Discussion and Conclusion

In this paper, we have used numerical techniques to study the roles of the Brinkman viscosity, the Darcy coefficient, and the coefficient of nonlinearity on the evolution of poroacoustic signals under the weakly-nonlinear model given in (3.9a). A finite difference scheme was constructed. We conducted a parameter study on the problem and discussed the implication to the creation or inhibiting of blow-ups. Finally, a perturbation analysis was carried out, reinforcing our numerical results for small $\epsilon\beta$. Due to the near perfect match to the perturbation results, we have high confidence in the numerical scheme and parameter study.

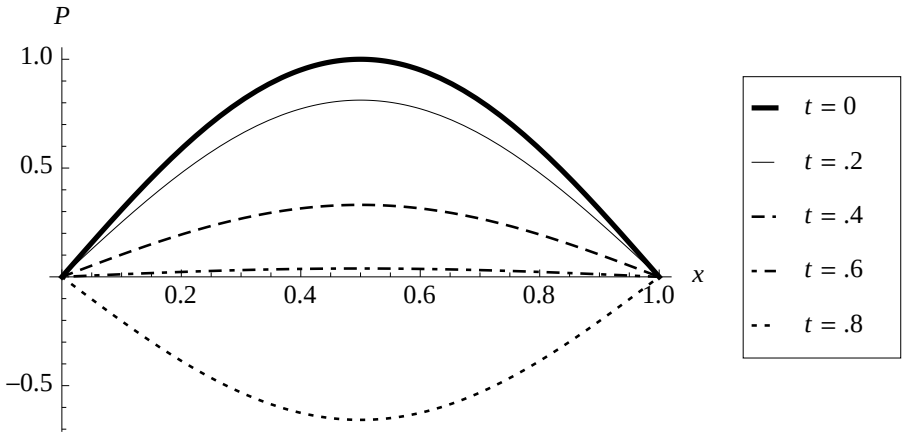

(a) Numerical.

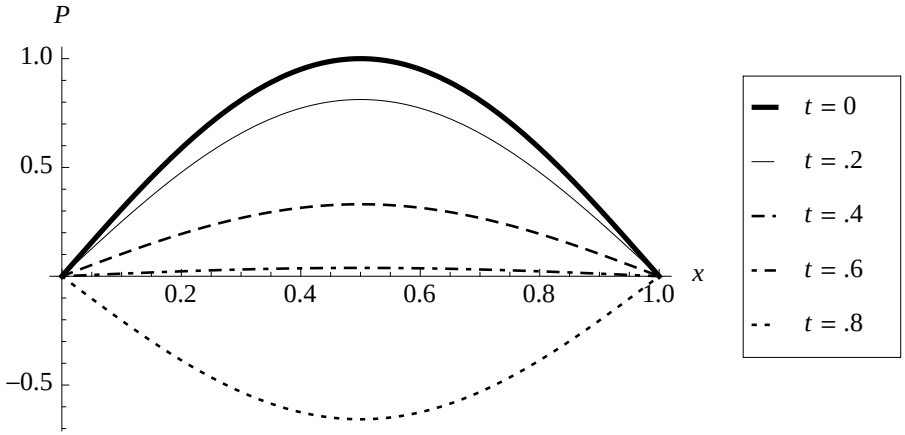

(b) Perturbation.

Figure 3.7: P vs x at various times for $\epsilon = 0.01$, $\delta = 0.05$, $\chi = 0.9$, $\beta = 3.625$, and $Re = 50$.

Based on these analyses, we report the following:

1. As can be seen from Figure 3.3, the Darcy term acts as a damping term for the wave equation. A larger δ leads to faster damping of the signal.

2. The Brinkman term, like the Darcy term, acts to decay the signal. However, for low Re, this decay is diffusive in nature, decaying very quickly to zero, unlike the damped oscillatory behavior of the Darcy case, as shown by the solid curve of Figure 3.4.

3. As Re is increased, the Brinkman term decreases in strength, giving rise to a transition

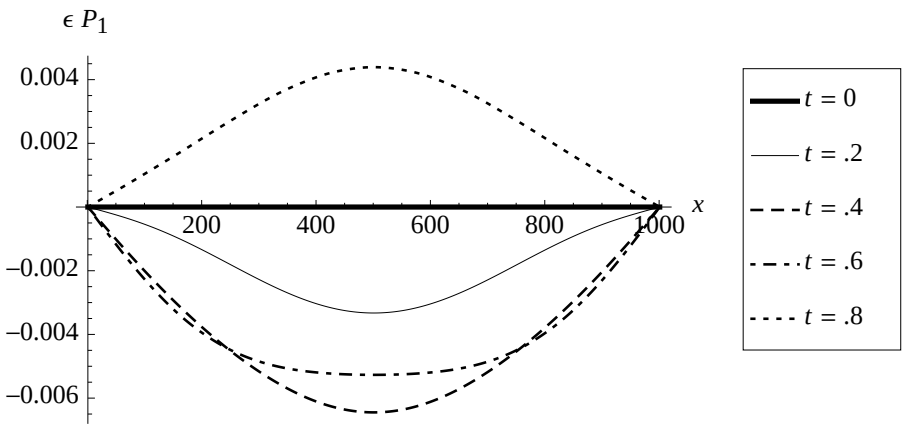

(a) Numerical.

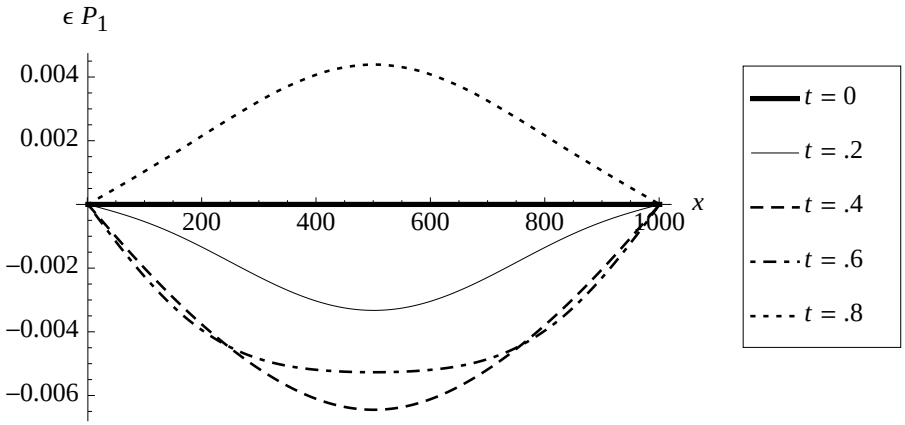

(b) Perturbation.

Figure 3.8: ϵP_1 vs x at various times for $\epsilon = 0.01$, $\delta = 0.05$, $\chi = 0.9$, $\beta = 1.077$, and $Re = 50$.

from a diffusive solution to a damped wave solution (Figure 3.4, dashed and dotted curves)

4. The nonlinear term gives rise to acoustical blow-ups. The time for these blow ups, as is evident in Figures 3.5(a) and 3.5(c), depends on the strength of the nonlinear term. For instance, Table 3.1 shows that for $\delta = 0.005$, smaller nonlinearities, those with $\epsilon\beta < 0.30$ show no signs of blow-ups, whereas when $\epsilon\beta > 0.40$, blow-ups occur relatively quickly, as seen in Figure 3.5(c).

5. Table 3.1 shows that the Darcy term helps mitigate blow-ups. As δ is increased, the Darcy term competes with the nonlinear term, shifting the blow-ups to later times. When the Darcy term is sufficiently large, the damping is fast enough to prevent the blow-ups from forming. For example, increasing δ from .005 to 0.05 with $\epsilon\beta = .40$ prevents the blow-up from forming, as in Figures 3.5(c) and 3.5(e).

6. The Brinkman term, when Re is small, forbids the formation of blow-ups, as can be seen in Figure 3.5. Increasing $\epsilon\beta$ shows very little effect on the evolution of the signal. However, as Re is increased, the equation transitions into a hyperbolic type equation and the damped oscillatory nature of the solution becomes dominant, allowing for blow-ups to occur. Table 3.2 shows that while in this hyperbolic regime, reducing Re shifts the blow-ups to later times, as in the Darcy case.

CHAPTER IV

Nonlinear Standing Waves Under Brinkman's Model

4.1 Introduction

In order to gain insight into the formation and evolution of nonlinear standing waves under the Brinkman model, a numerical analysis is conducted on the weakly nonlinear model studied thus far in this thesis. We develop a finite difference scheme and conduct a parameter study. An examination of the Brinkman, Darcy, and nonlinear terms is carried out in the context of their roles on shock formation. Finally, we compare our findings to those of previous results found in similar nonlinear equations found in other fields.

4.2 Mathematical Formulation and Problem Statement

As in *Rossmanith and Puri* (2014), we obtain the basic governing equation for a weakly-nonlinear model based on (1.2). Assuming 1D flow, conservation of mass, conservation of momentum, and the quadratic approximation to the isentropic equation of state *Wei and Jordan* (2013) take the form:

$$\varrho_t + (\varrho u)_x = 0, \tag{4.1}$$

$$\varrho(u_t + uu_x) = -\mathcal{P}_x + \tilde{\mu}\chi u_{xx} - \left(\frac{\mu\chi}{K}\right) u, \tag{4.2}$$

$$\mathcal{P} = \mathcal{P}_e + \varrho_e {c_e}^2 [s + (\beta - 1)s^2], \tag{4.3}$$

where ϱ is mass density and u is the velocity. Here and henceforth, we will use the notation $\eta_i{:=}\partial\eta/\partial i$, where η is a general variable. Note that the subscript e denotes the (constant) equilibrium state, c is the adiabatic speed of sound, β is the coefficient of nonlinearity, and $s = (\varrho - \varrho_e)/\varrho_e$ is the condensation.

From these equations, eliminating $\mathcal{P}$ from (4.2) using (4.3) we get,

$$\varrho(u_t + uu_x) = -\varrho_e {c_e}^2[s + (\beta - 1)s^2]_x + \tilde{\mu}\chi u_{xx} - \left(\frac{\mu\chi}{K}\right)u. \tag{4.4}$$

We now introduce the following dimensionless quantities, noting that $u = \phi_x$, where $\phi = \phi\,(x,t)$ is the velocity potential:

$$\begin{aligned} \phi^\diamond = \frac{\phi}{VL}, \quad u^\diamond = \frac{u}{V}, \quad x^\diamond = \frac{x}{L}, \\ t^\diamond = \frac{tc_e}{L}, \quad P^\diamond = \frac{\mathcal{P} - \mathcal{P}_e}{\varrho_e c_e V}. \end{aligned} \tag{4.5}$$

Here, V and L are the characteristic speed and length, both positive, respectively. Also, by introducing the Mach number $\epsilon = V/c_e$, and after further manipulation as well as using the binomial expansion approximation, dropping all terms of order $\mathcal{O}(\epsilon^2)$, we obtain *Jordan* (2009):

$$\Box^2\phi + \chi(Re)^{-1}\phi_{txx} - \delta\phi_t = \epsilon\partial_t[(\beta - 1)\phi_t^2 + \phi_x^2], \tag{4.6}$$

where $\Box^2 \equiv \partial_{xx} - \partial_{tt}$ is the 1D d'Alembertian operator, $Re = c_e L\sigma_e/\mu$, is a Reynolds number, $\delta \propto \chi$ is the dimensionless Darcy coefficient, and we have dropped the diamond superscripts on the dimensionless quantities. After some further manipulation, we arrive at:

$$\Box^2\phi + \chi(Re)^{-1}\phi_{txx} - \delta\phi_t = 2\epsilon(\beta - 1)\phi_t\phi_{tt} + 2\epsilon\phi_x\phi_{xt}. \tag{4.7}$$

(4.7) along with the following boundary and initial conditions, defines our initial-boundary-

value problem (IBVP):

$$\Box^2\phi + \chi(Re)^{-1}\phi_{txx} - \delta\phi_t = 2\epsilon(\beta-1)\phi_t\phi_{tt} + 2\epsilon\phi_x\phi_{xt}, \tag{4.8a}$$

$$\phi(x,0) = 0, \quad \phi_t(x,0) = 0, \quad for \quad (0 < x < 1) \tag{4.8b}$$

$$\phi(0,t) = \sin(\omega t), \quad \phi(1,t) = 0, \quad for \quad (t > 0). \tag{4.8c}$$

4.3 Numerical Analysis

4.3.1 Finite Difference Scheme Construction

With the IBVP having been stated, we will now make use of a finite difference scheme to find a numerical solution, meaning (4.8) must be discretized. The first step is to select the integers $I \geq 2$ and $J \geq 2$. Next, we set $\Delta x = T/I$ and $\Delta t = T/J$, where Δx and Δt denote uniform spatial and temporal step sizes, and T is the value of t for which the solution is sought. This gives the mesh points $x_i = i(\Delta x)$, for all $i = 0,1,...,I$, and $t_j = i(\Delta t)$, for all $j = 0,1,...,J$.

With this done, we will discretize (4.8a). We will start by replacing the second order derivatives with centered difference quotients, and first order derivatives with a backwards-Euler quotient. With these replacements, we obtain the difference equation,

$$\begin{aligned} \frac{\phi_{i+1}^j - 2\phi_i^j + \phi_{i-1}^j}{\Delta x^2} - \frac{\phi_i^{j+1} - 2\phi_i^j + \phi_i^{j-1}}{\Delta t^2} + \\ \frac{\chi}{Re}\left[\frac{(\phi_{i+1}^j - 2\phi_i^j + \phi_{i-1}^j) - (\phi_{i+1}^{j-1} - 2\phi_i^{j-1} + \phi_{i-1}^{j-1})}{\Delta x^2 \Delta t}\right] - \\ \delta\left(\frac{\phi_i^j - \phi_i^{j-1}}{\Delta t}\right) = \\ 2\epsilon\,(\beta-1)\left[\left(\frac{\phi_i^j - \phi_i^{j-1}}{\Delta t}\right)\left(\frac{\phi_i^{j+1} - 2\phi_i^j + \phi_i^{j-1}}{\Delta t^2}\right)\right] + \\ 2\epsilon\left[\left(\frac{\phi_i^j - \phi_i^j - 1}{\Delta x}\right)\left(\frac{\phi_i^j - \phi_{i-1}^j - \phi_i^{j-1} + \phi_{i-1}^{j-1}}{\Delta t \Delta x}\right)\right], \end{aligned} \tag{4.9}$$

where $P_i^j \approx P(x_i,t_j)$. Solving for the most advanced time step P_i^{j+1}, we obtain, after some

manipulation, the explicit scheme:

$$\begin{aligned}
&\phi_i^{j+1} = \\
&\Delta t \frac{\chi}{Re}\left(\frac{\phi_{i-1}^{j-1} - \phi_{i-1}^{j} - 2\phi_i^{j-1} + 2\phi_i^j + \phi_{i+1}^{j-1} - \phi_{i+1}^j}{\Delta x^2(2\epsilon\beta\phi_i^j - 1)}\right) + \\
&\Delta t^2\left(\frac{-\phi_{i-1}^j - 2\phi_i^j - \phi_{i+1}^j}{\Delta x^2(2\epsilon\beta\phi_i^j - 1)}\right) + \Delta t\delta\left(\frac{-\phi_i^{j-1} + \phi_i^j}{2\epsilon\beta\phi_i^j - 1}\right) + \\
&\left(\frac{\phi_i^{j-1} - 2\phi_i^j + 2\epsilon\beta(-(\phi_i^{j-1})^2 + \phi_i^{j-1}\phi_i^j + (\phi_i^j)^2)}{2\epsilon\beta\phi_i^j - 1}\right).
\end{aligned} \tag{4.10}$$

The last step involves discretizing the initial and boundary conditions (4.8b) and (4.8c). For details on this straightforward process see *Burden and Faires* (1993). The resulting conditions are as follows:

$$\phi_i^0 = 0, \tag{4.11a}$$

$$\partial_t \phi_i^0 = 0, \tag{4.11b}$$

$$\phi_0^j = \sin(\omega t_j), \tag{4.11c}$$

$$\phi_I^j = 0. \tag{4.11d}$$

4.3.2 Parameter Study

4.3.2.1 Time

We now study the effects of δ, Re, and $\epsilon\beta$ on the formation of a standing wave. Figure 4.1 is a plot of U versus x at various times. Here, we have used $Re = 200$, $\delta = 0.1$, and $\epsilon\beta = 0.265$. After a very short time, seen in Figure 4.1(a), the signal has just reached the right side boundary and has not yet formed a standing wave. We can see some evidence of the nonlinearity in altering the shape of the signal away from its sinusoidal origin. Figure 4.1(b) shows the signal at a medium time. A standing wave is starting to develop, and we see the beginnings of a sawtooth behavior form. Finally, in Figure 4.1(c), the long time regime, the standing wave has now formed and stabilized, and we see a strong sawtooth behavior. We see

that, as time progresses, a standing wave can indeed form and remain stable. Furthermore, for a certain value of parameters, sawtooth behavior, or shock formation, can be seen in this model.

4.3.2.2 Nonlinearity

Our next study is that of the nonlinear term, in particular its role in causing this sawtooth behavior. It has been shown in *Rasmussen* (2009) that an equation with a nonlinearity similar to the present study gives rise to a standing shock. Figure 4.2 shows that an increase in the nonlinearity of the system leads to the formation of the sawtooth behavior. We plot U versus x for long time, $t = 2.8$, with low δ and Re. Figure 4.2(a) is plotted with low $\epsilon\beta$ and shows no sign of a steepening effect. We increase $\epsilon\beta$ to a moderate value in Figure 4.2(b) and further to a high value in Figure 4.2(c). It is quite clear from this series of figures that as $\epsilon\beta$ is increased, we get a steepening in our signal, eventually giving rise to a sawtooth behavior.

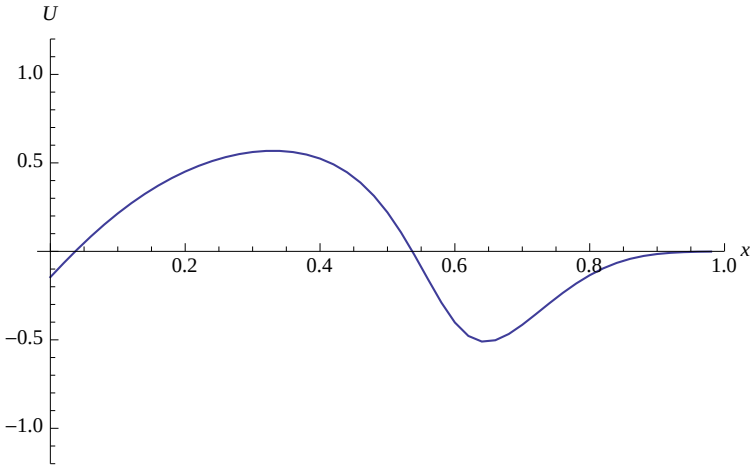

(a) $t = 0.4$.

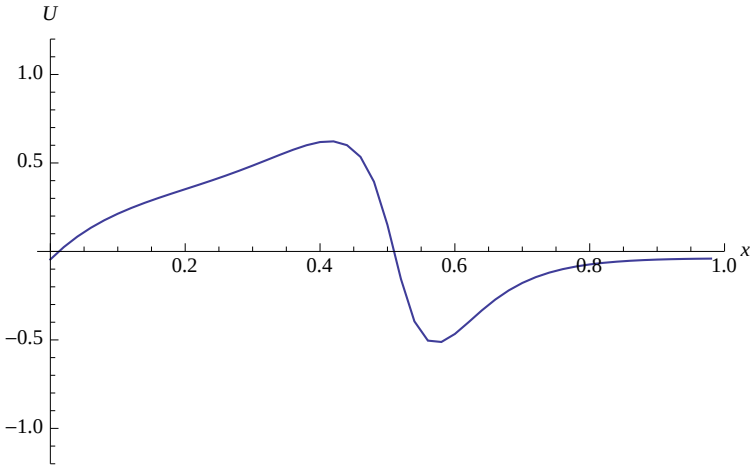

(b) $t = 1.4$.

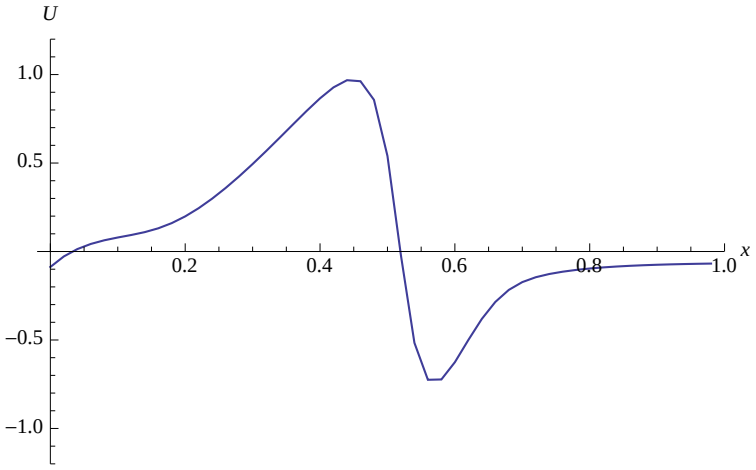

(c) $t = 2.8$.

Figure 4.1: U vs x for $\epsilon = 0.1$, $\beta = 2.65$, $\delta = 0.1$, $\chi = 0.9$, and $Re = 200$.

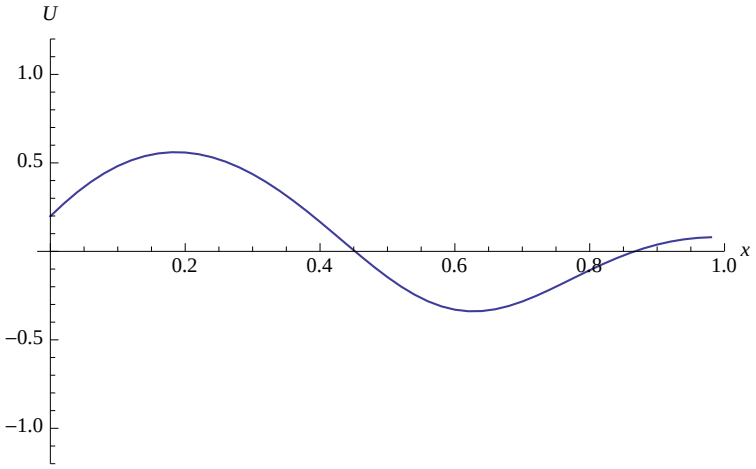

(a) $\epsilon\beta = 0.01077$.

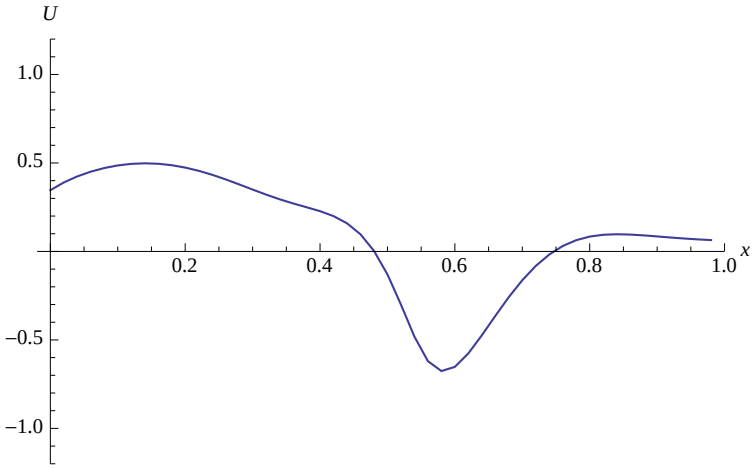

(b) $\epsilon\beta = 0.1077$.

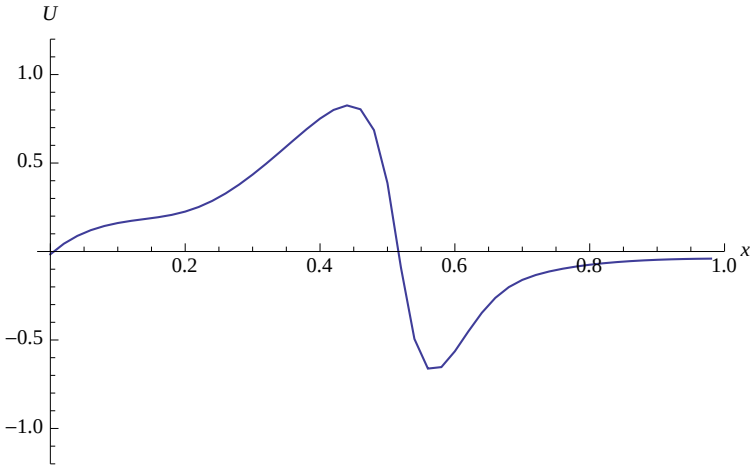

(c) $\epsilon\beta = 0.265$.

Figure 4.2: U vs x for $t = 2.8$, $\delta = 0.1$, $\chi = 0.9$, and $Re = 200$.

4.3.2.3 Darcy Term

We now study how the Darcy term affects this sawtooth behavior.. Setting $Re = 200$, $\epsilon\beta = .265$, and $t = 2.8$, we plot Figure 4.3. A low value of δ is plotted in Figure fig4.3a. We see the sawtooth behavior from the nonlinearity has occurred. A medium value of δ, as plotted in Figure 4.3(b), has reduced the amplitude of the signal, and in so doing has begun to mitigate the steepening effect of the nonlinearity. Figure 4.3(c) shows that with very high δ, the amplitude is reduced further, while the remnants of the sawtooth behavior are still noted. This leads to the conclusion that the Darcy term acts to dampen the signal, reducing the amplification which occurs in closed, driven systems, and reducing the ability for shock formation.

4.3.2.4 Brinkman Term

We will use a similar technique to study the role of the Brinkman term, by setting $\delta = .1$, $\epsilon\beta = .265$, and $t = 20$. The results are plotted in Figure 4.4. Beginning with the high Reynolds number case in Figure 4.4(a), we find the sawtooth behavior seen before. We decrease Re (increasing the strength of the Brinkman term) and plot the result in Figure 4.4(b). The amplitude of the signal has decreased, and the sawtooth behavior has been significantly reduced. In Figure 4.4(c), the low Re case, the amplitude is further reduced, and the effects of the nonlinearity have been masked. It is quite clear from this series of figures that the Brinkman term is a diffusive term, acting to reduce the amplitude of the signal and prevent shock formation.

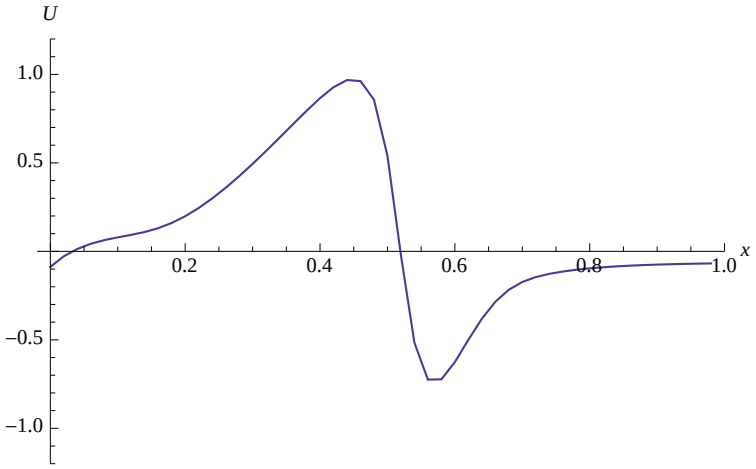

(a) $\delta = 0.01$.

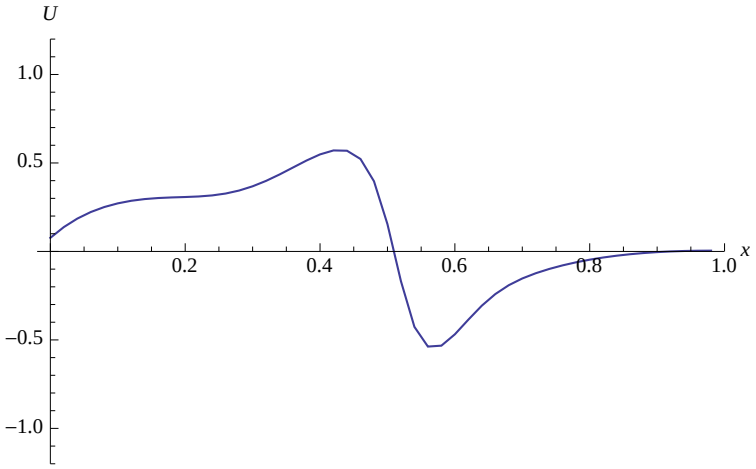

(b) $\delta = 0.3$.

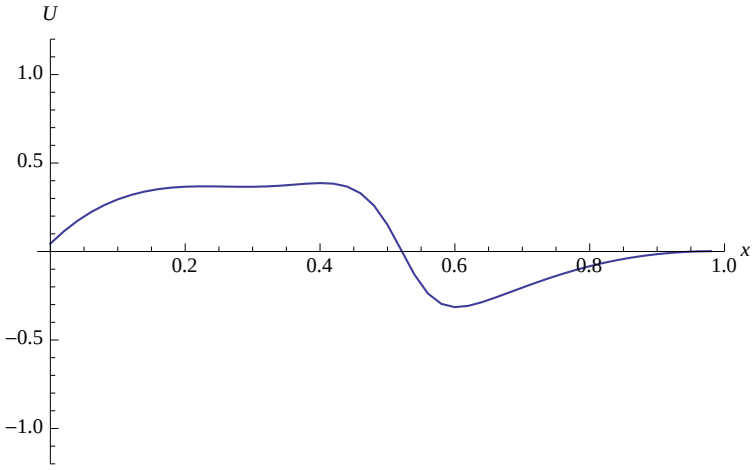

(c) $\delta = 0.8$.

Figure 4.3: U vs x for $t = 2.8$, $\epsilon\beta = 0.265$, $\chi = 0.9$, and $Re = 200$.

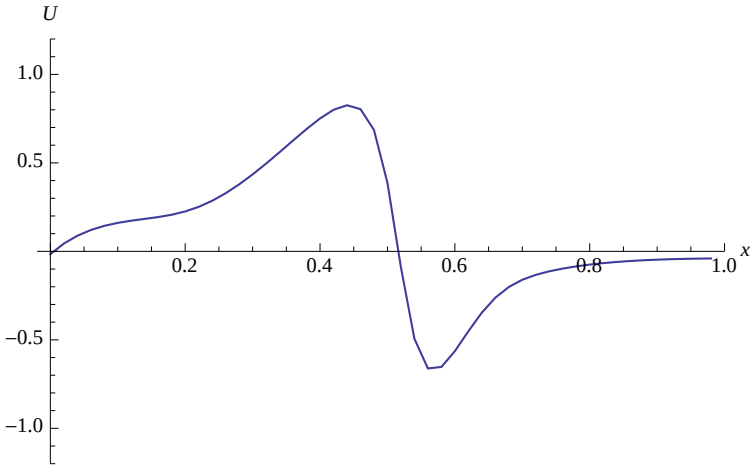

(a) $Re = 200$.

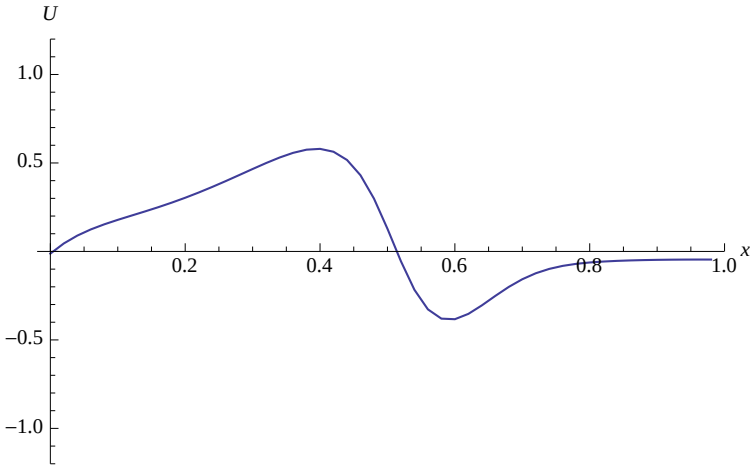

(b) $Re = 100$.

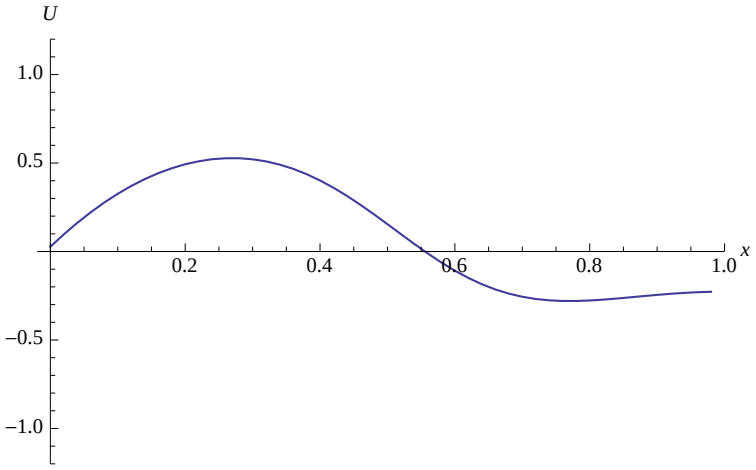

(c) $Re = 20$.

Figure 4.4: U vs x for $t = 2.8$, $\delta = 0.1$, $\chi = 0.9$, and $\epsilon\beta = 0.265$.

4.3.3 Previous Results

In order to build confidence in our numerical scheme, we plot Figure 4.5. This is a short time plot of the acoustic pressure, P, where $P = \partial_t \phi$, versus position. Here, we have set $\delta = 0$, and $Re = \infty$. We see that as time goes on, the wave front steepens significantly. *Jordan and Christov* (2005) studied a similar equation and found the same behavior. The nonlinearity causes a steepening in the pressure, giving rise to a shock formation. With this match, we can be confident in our numerical scheme.

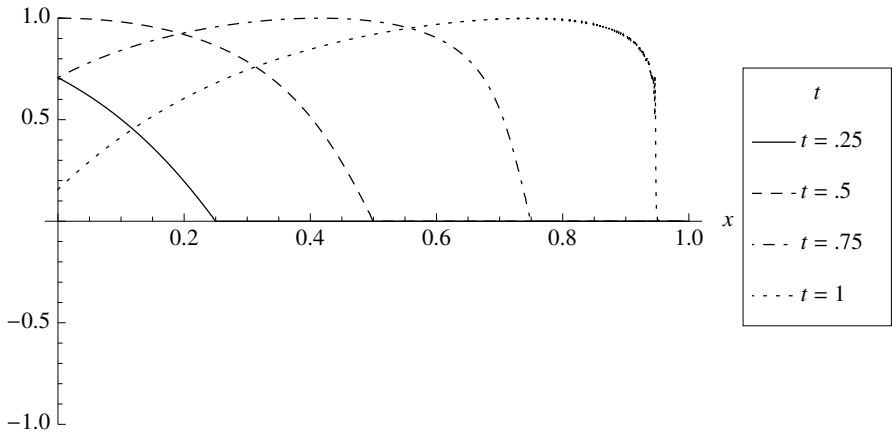

Figure 4.5: P vs x at various times for $\epsilon = 0.1$and $\beta = 2.65$, at $Re = 200$, and $\delta = 0.1$.

4.4 Discussion and Conclusion

In this chapter, we have used numerical techniques to study the roles of the Brinkman term, the Darcy coefficient, and the coefficient of nonlinearity on the formation of nonlinear standing waves under the weakly-nonlinear model given in (4.8). A finite difference scheme was constructed for this model. We conducted a parameter study on the problem and discussed the implications in the context of shock formation.

1. The Brinkman model (4.4) of poroacoustic propagation permits sawtooth behavior.

2. The origin of the sawtooth behavior is the nonlinear term, as can be seen in Figure

4.2. An increase in $\epsilon\beta$ causes a more prominent steepening in the signal. This increase also gives rise to an increase in the amplification of the signal. With a very high value of $\epsilon\beta$, the signal will eventually blow up.

3. Figure 4.3 shows that the Darcy term dampens the signal amplitude, reducing the effective steepening in the signal, and thus reducing the sawtooth behavior.

4. The Brinkman term, being a diffusive term, also lowers the signal amplitude. It can be seen from Figure 4.4 that it significantly reduces the steepening caused by the nonlinearity, forbidding the formation of the sawtooth behavior for low Re values.

5. As was found in similar equations without the Darcy and Brinkman terms, this model of poroacoustics also shows shock formation in the small time regime, as seen in Figure 4.5.

CHAPTER V

A Recasting of Brinkman's Equation as the Damped Burgers Equation

5.1 Introduction

In order to gain a better understanding of the behavior of finite-amplitude harmonic waves under a Brinkman-type poroacoustic model, we make use of approximations and transformations to recast our equation into the damped Burgers equation. We examine two special solutions of the damped Burgers equation: the approximate solution to the damped Burgers equation and the boundary value problem given an initial sinusoidal signal. We study the effects of the Darcy coefficient, Reynolds number, and nonlinear coefficient on these solutions.

5.2 Mathematical Formulation

We begin with the Brinkman equation from *Jordan* (2009), as well as *Rossmanith and Puri* (2014)-*Rossmanith and Puri* (2016):

$$\Box^2\phi + \chi(Re)^{-1}\phi_{txx} - \delta\phi_t = \epsilon\partial_t[(\beta-1)\phi_t^2 + \phi_x^2]. \tag{5.1}$$

Here, $\Box^2 \equiv \partial_{xx} - \partial_{tt}$ is the 1D d'Alembertian operator, $\phi = \phi\ (x,t)$ is the velocity potential, $Re = c_e L\sigma_e/\mu$, is a Reynolds number, $\delta \propto \chi$ is the dimensionless Darcy coefficient, ϵ is the mach number, and β is the coefficient of nonlinearity.

Crighton (1979) has shown that the unidirectional approximation (right running) on a model equation of nonlinear acoustics gives rise to the classical Burgers equation. More recently, *Jordan* (2016) asserted that applying the right running unidirectional approximation to (5.1) allows it to be recast as the damped Burgers equation (DBE). To verify this assertion, we rewrite the operator form of the d'Alembertian in (5.1) to get:

$$(\partial_x + \partial_t)(\partial_x - \partial_t)\phi + \chi(Re)^{-1}\phi_{txx} - \delta\phi_t = \epsilon\partial_t[(\beta - 1)\phi_t^2 + \phi_x^2]. \tag{5.2}$$

Assuming right-running waves and employing the approximation $\phi_x \propto$ -ϕ_t in the small terms of (5.2), yields:

$$(\partial_x + \partial_t)(-2\partial_t)\phi + \chi(Re)^{-1}\phi_{txx} - \delta\phi_t = 2\epsilon\beta\phi_t\phi_{tt}. \tag{5.3}$$

We then integrate equation (5.3) with respect to t to get:

$$-2(\partial_x + \partial_t)\phi + \chi(Re)^{-1}\phi_{xx} - \delta\phi = \epsilon\beta(\phi_t)^2. \tag{5.4}$$

Differentiating equation (5.4) with respect to x and rearranging, we arrive at:

$$u_t + (1 + \epsilon\beta u)\, u_x - \frac{1}{2}\chi(Re)^{-1}u_{xx} + \frac{1}{2}\delta u = 0. \tag{5.5}$$

Here, we have used the fact that $\phi_x = u$. We set $\hat{x} = x$ - t and $\hat{t} = t$, which reduces (5.3) to

$$u_{\hat{t}} + \epsilon\beta u u_{\hat{x}} - \frac{1}{2}\chi(Re)^{-1}u_{\hat{x}\hat{x}} + \frac{1}{2}\delta u = 0, \tag{5.6}$$

which is the DBE.

In the following section, we will study the approximate traveling wave solution to (5.6),

and discuss the role of the Darcy, Brinkman, and nonlinear terms on the behavior of the solution. In section 4, we will analyze numerically the damped form of Cole's problem *Cole* (1951). We will also analytically derive an approximate solution to (5.6) from an energy analysis. Lastly, in section 5, we relate our study to previous results in other fields.

5.3 Traveling Wave Solution

In order to derive an approximate traveling wave solution for (5.1), we transform (5.6) into its more widely used form. We begin by letting $\bar{x} = \sqrt{(2Re/\chi)}\ \hat{x}$. This gives:

$$u_{\hat{t}} + \epsilon\beta\sqrt{\frac{2Re}{\chi}}uu_{\bar{x}} - u_{\bar{x}\bar{x}} + \frac{1}{2}\delta u = 0. \tag{5.7}$$

Now, defining $\alpha = \epsilon\beta\sqrt{(2Re/\chi)}$ and $\hat{u} = \alpha\ u$, and after some manipulation we get,

$$\hat{u}_{\hat{t}} + \hat{u}\hat{u}_{\bar{x}} - \hat{u}_{\bar{x}\bar{x}} + \lambda\hat{u} = 0, \tag{5.8}$$

where $\lambda = \delta/2$. We make use of the approximate solution found by *Malfiet* (1993):

$$\hat{u} = 2e^{-\lambda\hat{t}}[(1-y)(1 + a_3y^3(1+y) + a_5y^5(1+y)...], \tag{5.9}$$

where:

$$\begin{aligned} y &= \tanh[\bar{x} - \frac{2}{\lambda}(1 - e^{-\lambda\hat{t}})], \\ a_3 &= \frac{1}{3}(e^{-\lambda\hat{t}} - 1), \\ a_5 &= -\frac{1}{60}(\lambda e^{-\lambda\hat{t}} + 8e^{-2\lambda\hat{t}} - 40e^{-\lambda\hat{t}} + 32). \end{aligned}$$

Figure 5.1 is a plot of $\hat{u}$ vs $\hat{x}$ for various values of lambda. Plotting $\hat{u}$ instead of u effectively normalizes the amplitude across all studies. This allows us to more clearly see

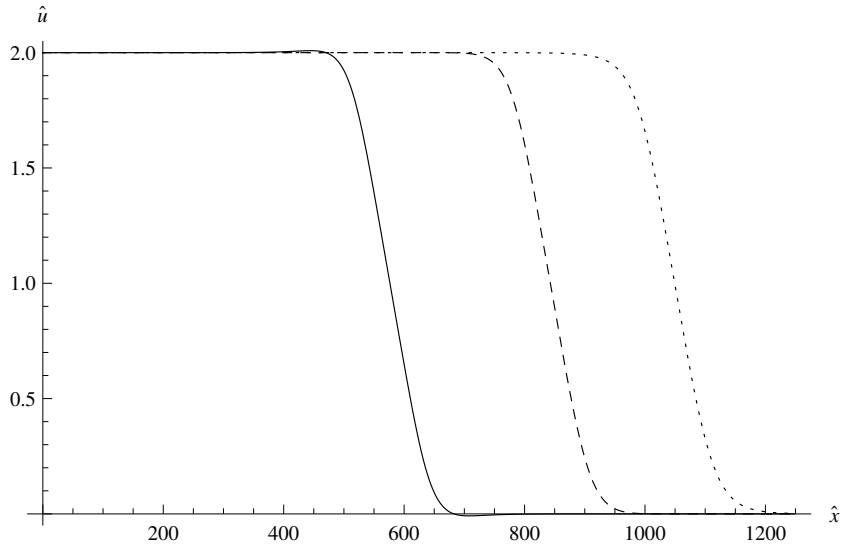

Figure 5.1:
$\hat{u}$ vs $\hat{x}$ with $\hat{t} = 10$, $Re = 2000$, $\chi = 0.9$, $\epsilon = 0.1$, and $\beta = 1.07$. Solid: $\lambda = 0.2$. Dashed: $\lambda = 0.1$. Dotted: $\lambda = 0.05$.

the effects that the various parameters have on the structure of the solution. It is clear that the location of the drop in wave amplitude is λ dependent. Increasing λ shifts the location to shorter distances. However, the form of the solution is unchanged. Next, we study the effects of Re on the wave.

We plot $\hat{u}$ vs $\hat{x}$ for various values of Re in Figure 5.2. It is clear that the location of the drop in wave amplitude is Re dependent. Increasing Re, which effectively reduces the strength of the Brinkman term, delays the location of the drop to larger distances. Unlike the λ dependence however, a prominent steepening in the wave form can be seen with decreasing Re.

In order to study the effects of β on the solution, we plot u vs $\hat{x}$ in Figure 5.3 instead of $\hat{u}$ vs $\hat{x}$, because the β dependence is found only in α. We note that the amplitude is decreased as a function of increasing β. The apparent steepening found in this figure is a result of the different starting amplitudes, rather than the structure of the solution.

We now wish to study the behavior of (5.1) using an initial sinusoidal signal.

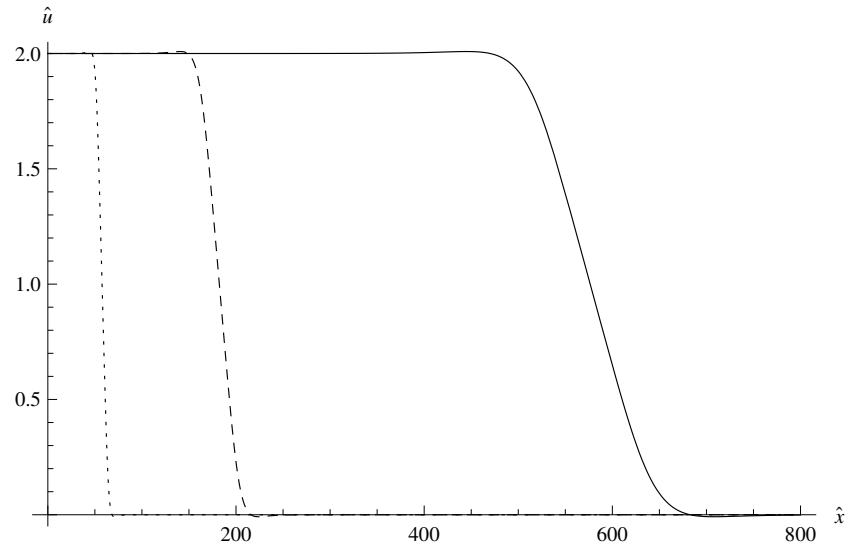

Figure 5.2:
$\hat{u}$ vs $\hat{x}$ with $\hat{t} = 10$, $\lambda = 0.2$, $\chi = 0.9$, $\epsilon = 0.1$, and $\beta = 1.07$. Solid: $Re = 2000$. Dashed: $Re = 200$. Dotted: $Re = 20$.

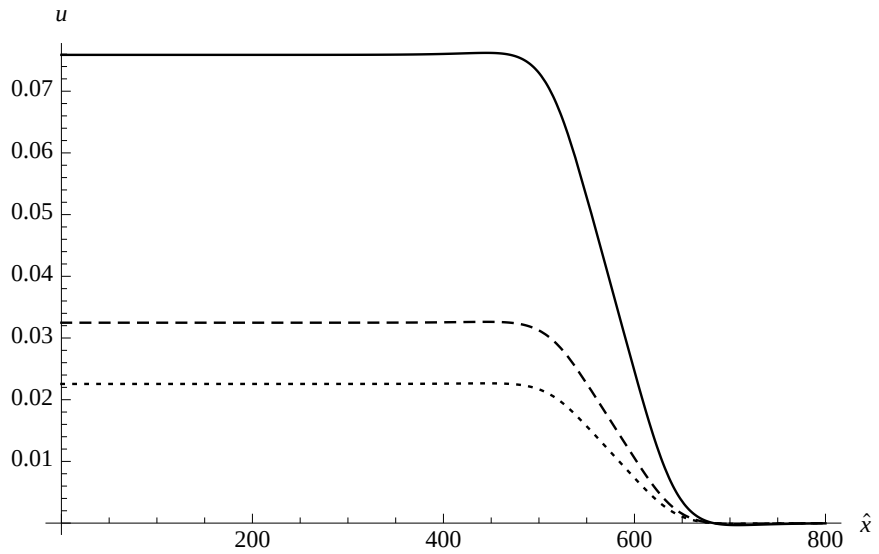

Figure 5.3:
u vs $\hat{x}$ with $\hat{t} = 10$, $\lambda = 0.2$, $\chi = 0.9$, $\epsilon = 0.1$, and $Re = 2000$. Solid: $\beta = 1.07$. Dashed: $\beta = 2.5$. Dotted: $\beta = 3.6$.

5.4 Sinusoidal Initial Condition: Cole's Problem

Starting with (5.6), we define $\tilde{x} = (\hat{x}/\epsilon\beta)$. This gives:

$$u_{\hat{t}} + uu_{\tilde{x}} - \frac{1}{2(\epsilon\beta)^2}\chi(Re)^{-1}u_{\tilde{x}\tilde{x}} + \frac{\delta}{2}u = 0. \tag{5.10}$$

Then, defining $\tilde{\nu} = \chi/[2Re(\epsilon\beta)^2]$ and $\lambda = \delta/2$, and dropping the Darcy term, we have the classical Burgers equation,

$$u_{\hat{t}} + uu_{\tilde{x}} - \tilde{\nu}u_{\tilde{x}\tilde{x}} = 0. \tag{5.11}$$

We now define the initial and boundary conditions:

$$u(0,\hat{t}) = u(1,\hat{t}) = 0, \quad for \quad \hat{t} > 0; \tag{5.12a}$$

$$u(\tilde{x},0) = \sin(\pi\tilde{x}), \qquad for \quad 0 < \tilde{x} < 1. \tag{5.12b}$$

The exact solution to this problem, as derived in *Cole* (1951), is,

$$u = 4\pi\tilde{\nu}\left[\frac{\sum_{n=1}^{\infty} ne^{-\tilde{\nu}n^2\pi^2\hat{t}}I_n\left(\frac{1}{2\pi\tilde{\nu}}\right)\sin(n\pi\tilde{x})}{I_0\left(\frac{1}{2\pi\tilde{\nu}}\right) + 2\sum_{n=1}^{\infty} e^{-\tilde{\nu}n^2\pi^2\hat{t}}I_n\left(\frac{1}{2\pi\tilde{\nu}}\right)\cos(n\pi\tilde{x})}\right], \tag{5.13}$$

where $I_h(\cdot)$ denotes the modified Bessel function of the first kind of order h.

We now study the role that the Darcy term plays by looking at the DBE:

$$u_{\hat{t}} + uu_{\tilde{x}} - \tilde{\nu}u_{\tilde{x}\tilde{x}} + \lambda u = 0. \tag{5.14}$$

We solve numerically the DBE (with the Darcy term) and compare the result to the exact solution to the undamped case (5.13). The results are plotted in Figure 5.4.

Here, we have u vs. $\tilde{x}$ plotted for various values of λ with $Re = 200$, and $\beta = 1.07$, which corresponds to CO_2 at several thousand Kelvin *Thompson* (1972). There is an excellent match to the exact solution for the $\lambda = 0$ case, giving confidence in the numerical scheme.

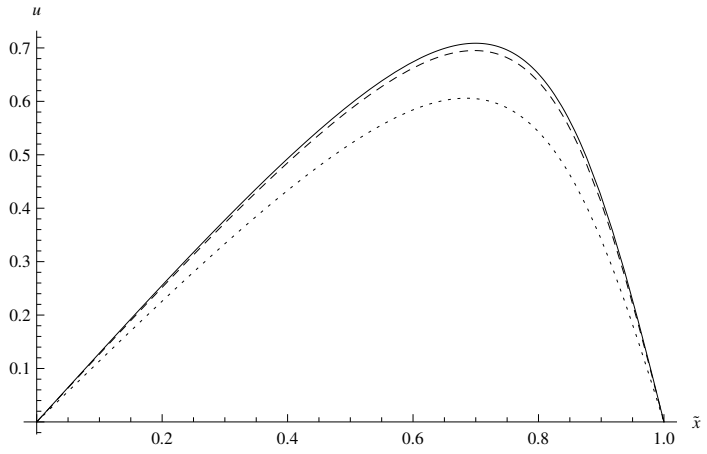

Figure 5.4:
u vs $\tilde{x}$ with $\hat{t} = .4$, $\beta = 1.07$, $\chi = 0.9$, $\epsilon = 0.1$, and $Re = 200$. Solid: $\lambda = 0$. Dashed: $\lambda = 0.05$. Dotted: $\lambda = 0.4$.

A drop in the signal's amplitude is noted as a function of increasing λ.

Next, to investigate how $\tilde{\nu}$ affects the evolution of the signal, we plot Figure 5.5. We see that increasing Re ($\tilde{\nu}$ is decreasing) gives rise to a steepening effect in time, leading to a blow-up for very small $\tilde{\nu}$. Also, the signal amplitude decays more slowly as a function of increasing Re.

In Figure 5.6, $\tilde{\nu}$ and $\hat{t}$ are kept constant, and the change in signal amplitude as a function of λ is studied. It is clear that λ is a damping term, reducing the amplitude with increasing λ. Furthermore, we see the prominent steepening effect $\tilde{\nu}$ has on the signal. λ reduces this steepening, slightly shifting the maximum of the signal towards center.

5.4.0.1 Energy Analysis

In order to develop a better understanding of (5.10), we will analyze its energy equation. We start by multiplying all terms in (5.10) by u giving:

$$uu_{\hat{t}} + u^2 u_{\tilde{x}} - \tilde{\nu} u u_{\tilde{x}\tilde{x}} + \lambda u^2 = 0. \tag{5.15}$$

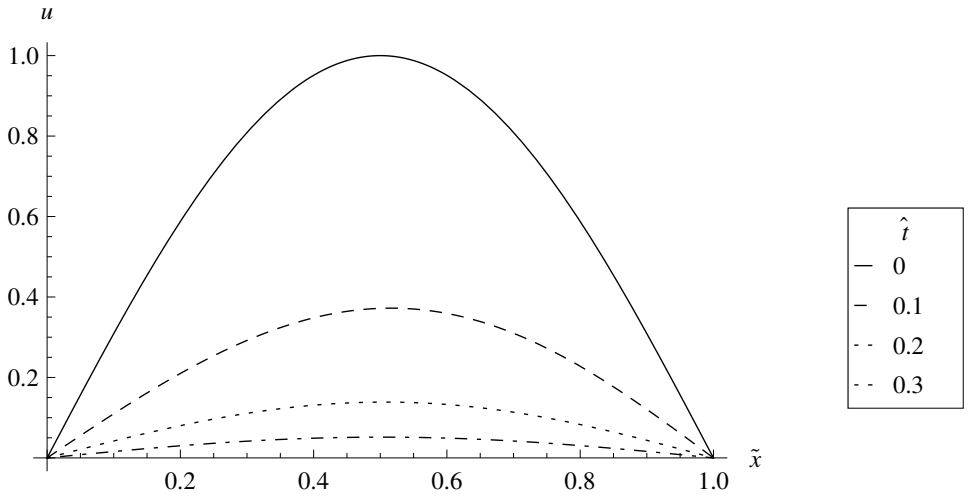

(a) $\tilde{\nu} = 1$.

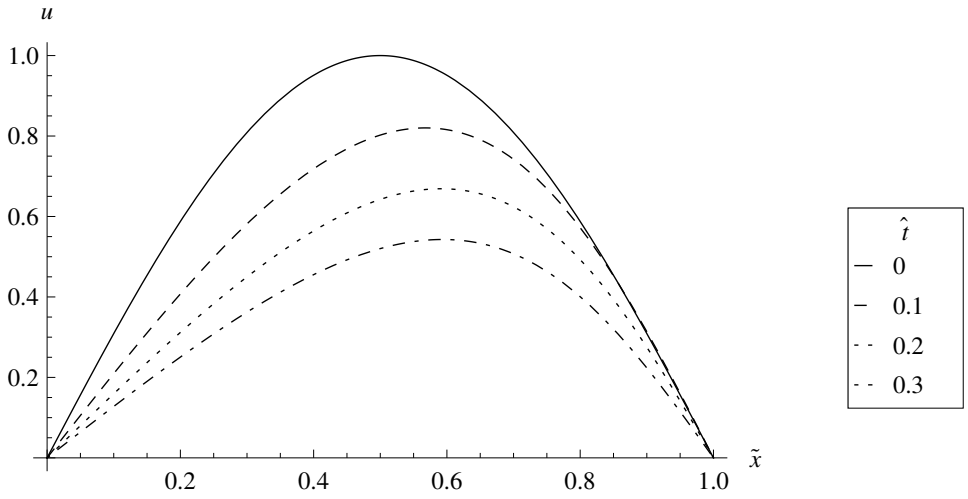

(b) $\tilde{\nu} = 0.2$.

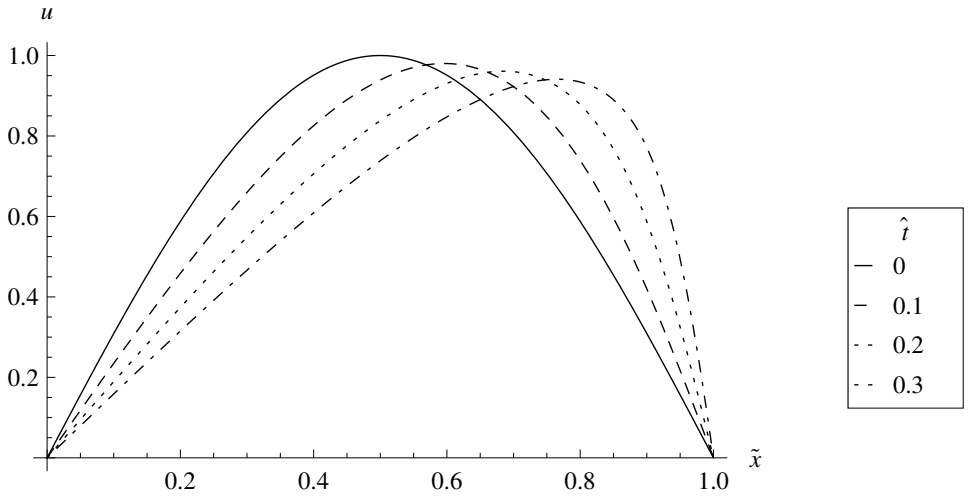

(c) $\tilde{\nu} = 0.02$.

Figure 5.5: u vs $\tilde{x}$ for various times with $\lambda = .001$, $\epsilon = 0.1$, $\beta = 1.07$.

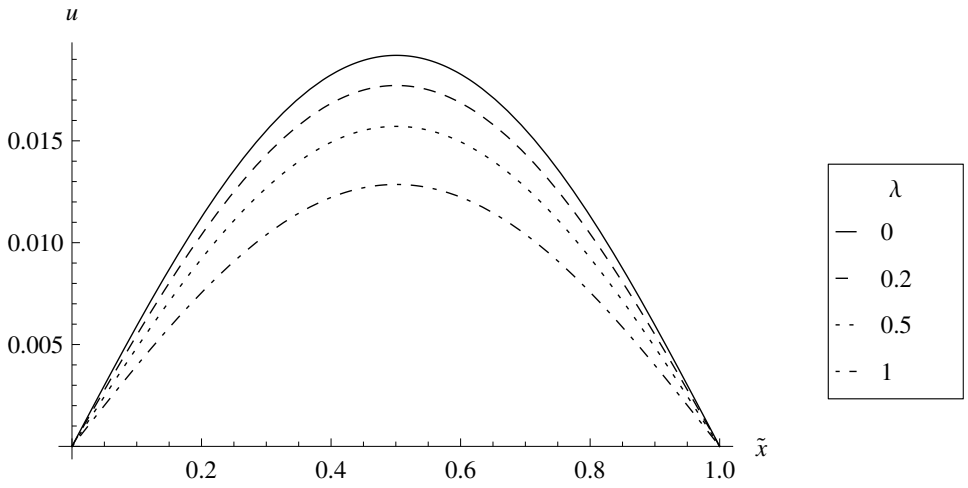

(a) $\tilde{\nu} = 1$.

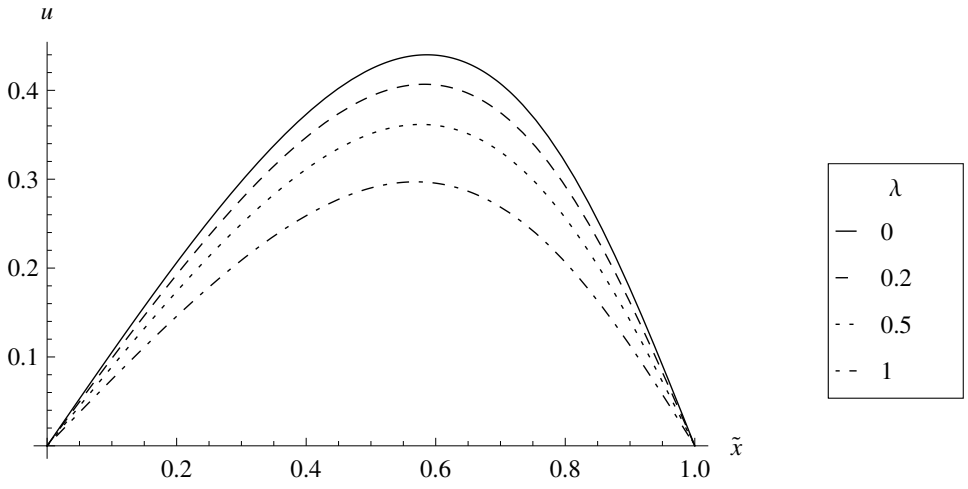

(b) $\tilde{\nu} = 0.2$.

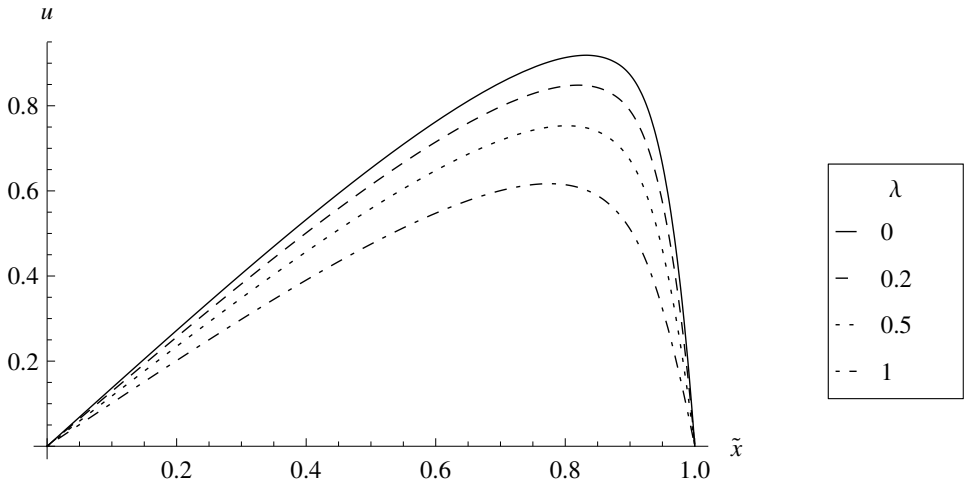

(c) $\tilde{\nu} = 0.02$.

Figure 5.6: u vs $\tilde{x}$ for various λ with $\epsilon = 0.1$, $\beta = 1.07$, $\hat{t} = 0.4$.

Next, integrating (5.15) over the spatial domain results in:

$$\frac{d}{d\hat{t}}\left(\frac{1}{2}\int_{\tilde{x}_1}^{\tilde{x}_2}(u^2)d\tilde{x}\right)+\frac{1}{3}[u^3(\tilde{x}_2,\hat{t})-u^3(\tilde{x}_1,\hat{t})]+\lambda\int_{\tilde{x}_1}^{\tilde{x}_2}u^2d\tilde{x}= \\ \tilde{\nu}(u\partial_{\tilde{x}}u)\Big|_{\tilde{x}_1}^{\tilde{x}_2}-\tilde{\nu}\int_{\tilde{x}_1}^{\tilde{x}_2}(\partial_{\tilde{x}}u)^2. \tag{5.16}$$

Following the energy analysis of the undamped Burger's equation found in *Cole* (1951), the physical significance of the terms in (5.16) are as follows:

$$\begin{aligned}
\frac{d}{d\hat{t}}\left(\frac{1}{2}\int_{\tilde{x}_1}^{\tilde{x}_2}(u^2)d\tilde{x}\right) &= \text{total rate of change of kinetic energy in the system,}\\
\frac{1}{3}[u^3(\tilde{x}_2,\hat{t})-u^3(\tilde{x}_1,\hat{t})] &= \text{net flux of kinetic energy out across the boundaries,}\\
\lambda\int_{\tilde{x}_1}^{\tilde{x}_2}u^2d\tilde{x} &= \text{dissipation by pore interaction,}\\
(u\partial_{\tilde{x}}u)\Big|_{\tilde{x}_1}^{\tilde{x}_2} &= \text{rate of work done on the system at the boundaries,}\\
\tilde{\nu}\int_{\tilde{x}_1}^{\tilde{x}_2}(\partial_{\tilde{x}}u)^2 &= \text{total dissipation of energy by viscosity.}
\end{aligned}$$

It is worth noting that the pore interaction term is a new contribution made by the Darcy term.

For our particular study, we recast (5.16) and make use of our particular boundary conditions to give:

$$\left(\frac{d}{d\hat{t}}+2\lambda\right)K=-\tilde{\nu}\int_0^1(\partial_{\tilde{x}}u)^2, \tag{5.17}$$

where $K=(1/2)\int_0^1(u^2)d\hat{x}$ is the kinetic energy. Noting that $\left(\frac{d}{d\hat{t}}+2\lambda\right)$ is the relaxation operator, which admits an exponential kernel, the following ansatz is suggested:

$$u=e^{-mt}\breve{u}, \tag{5.18}$$

where $\breve{u}$ denotes the solution of (5.11) given (5.12).

Applying (5.18) to (5.17) we get,

$$\frac{d}{d\hat{t}}K + (2\lambda - 2m)K = -\tilde{\nu}\int_0^1 (\partial_{\tilde{x}}\breve{u})^2, \tag{5.19}$$

which is exactly the energy equation for the classical Burgers equation when $m = \lambda$. Thus, (5.18) satisfies the energy equation (5.17).

Unfortunately, our ansatz does not solve the DBE. However, it does provide a practical approximation. Applying (5.18) to the DBE (5.14) results in,

$$\breve{u}_{\hat{t}} + \breve{u}\breve{u}_{\tilde{x}} - \tilde{\nu}\breve{u}_{\tilde{x}\tilde{x}} = -(e^{\lambda\hat{t}} - 1)\breve{u}\breve{u}_{\tilde{x}}. \tag{5.20}$$

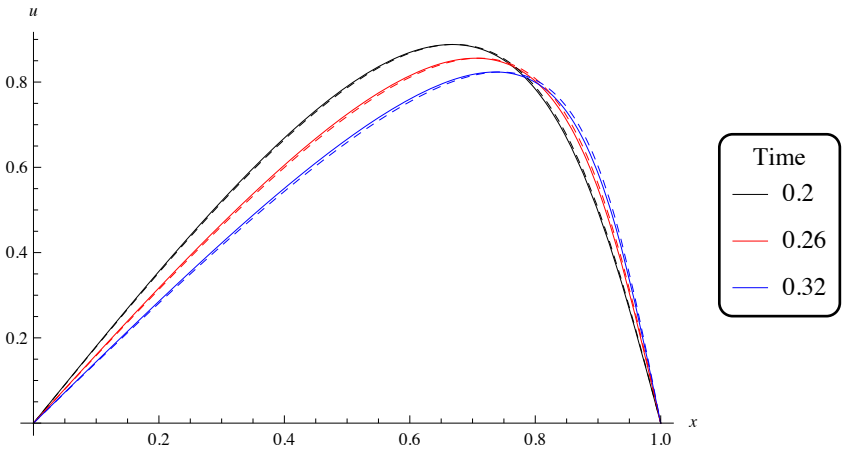

Figure 5.7: u vs $\tilde{x}$ with $\tilde{\nu} = 0.039$, $\lambda = 0.2$. Solid: Numerical DBE solution. Dashed: Approximate analytical solution.

The lefthand side of (5.20) is zero from (5.11). Thus, this solution approximately satisfies the DBE when $\hat{t} \ll 1/\lambda$. Figure 5.7 is a comparison of the numerical solution to the DBE and the approximate solution (5.18). We see that the approximate solution fits very well for small times. However, Figure 5.8 shows that when $\hat{t}$ is of the order $1/\lambda$, this approximate

solution does not hold.

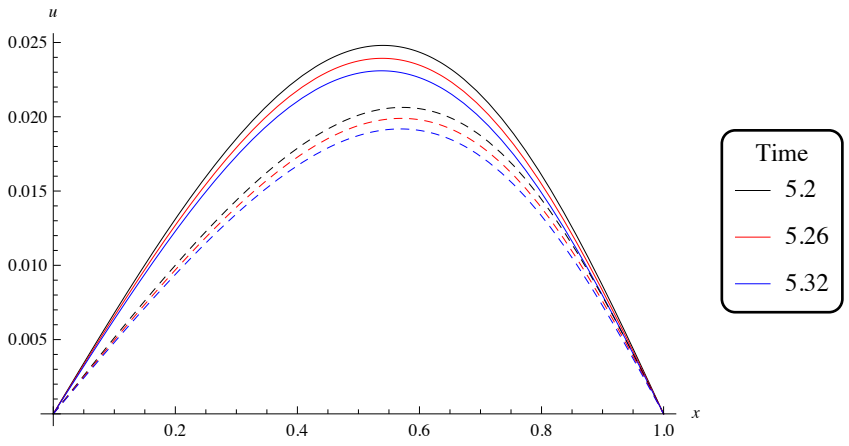

Figure 5.8: u vs $\tilde{x}$ with $\tilde{\nu} = 0.039$, $\lambda = 0.2$. Solid: Numerical DBE solution. Dashed: Approximate analytical solution.

5.5 Relation to Other Fields

Korsunskii (1991) found an approximate solution to (5.14) in relation to magnetoacoustic waves in an electrically conducting fluid. For $\lambda \ll 1$, he found that the approximate solution, bounded in the limit $\tilde{x} \to \infty$, can be written in the form :

$$\hat{u} = e^{\lambda \hat{t}} \left[D - A \tanh \left(\frac{A e^{-\lambda \hat{t}}}{2\tilde{\nu}} \left(\tilde{x} - D \frac{1 - e^{-\lambda \hat{t}}}{\lambda} \right) \right) \right], \tag{5.21}$$

where A and D are constants. This approximate solution is valid for $\hat{t} < 1/\lambda$.

We compare the solution in (5.21) with our numerical solution in Figure 5.9. We have used a low value of $\lambda = 0.05$ and a time of $t = 7$. We find a close match to our numerical work.

Soluyan and Khokhlov (1962) studied a similar equation in the context of relaxing media.

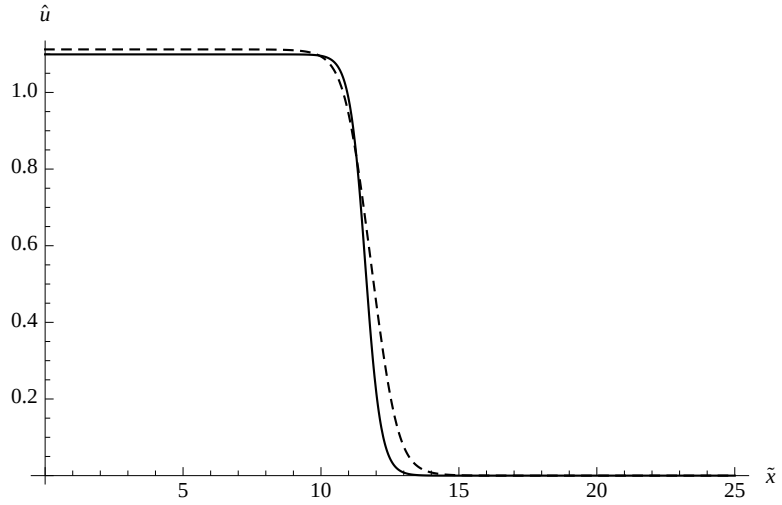

Figure 5.9: $\hat{u}$ vs $\tilde{x}$ with $\chi = 0.9$, $Re = 100$, $\hat{t} = 7$, $\epsilon = 0.1$, $\beta = 1.7$, $\lambda = 0.05$, $A = 0.8$, and $D = 0.8$. Solid: Numerical DBE solution. Dashed: Approximate analytical solution.

Beginning with (5.5) and dropping the Brinkman term, we get,

$$u_t + (1 + \epsilon\beta u)\, u_x + \frac{1}{2}\delta u = 0. \tag{5.22}$$

Now, replacing x with t, and vice-versa, as well as defining $\delta/2 = \lambda$, we have the inviscid damped Burgers equation found in *Soluyan and Khokhlov* (1962):

$$u_x + (1 + \epsilon\beta u)\, u_t + \lambda u = 0. \tag{5.23}$$

Soluyan found that the exact solution to (5.23) has the form,

$$\omega t = \arcsin(ue^{\lambda x}) + \frac{\epsilon\beta\omega}{\lambda}(1 - e^{-\lambda x})ue^{\lambda x} + \omega x, \tag{5.24}$$

where $\omega = \pi$ in the context of this study.

5.6 Discussion

In this paper, we have used analytical and numerical techniques to study the behavior of the right-running approximation to the Brinkman-based poroacoustic model given in (5.1); that is, we recast the Brinkman equation as the DBE and studied the roles of the Reynolds number, Darcy coefficient, and the nonlinear coefficient β under two special settings: the traveling wave solution, and the sinusoidal initial condition. Based on these analyses, we report the following:

5.6.1 Traveling Wave

1. As shown in Figure 5.1, the drop in wave amplitude is λ dependent. An increase in λ leads to a shift in the location of the drop of the signal amplitude to shorter distances.

2. We note that an increase in Re shifts the drop of the amplitude of the signal to larger distances, as shown in Figure 5.2. Also noted in Figure 5.2, increasing Re mitigates the steepness caused by the nonlinearity.

3. The nonlinear term allows for a steepening effect. However, this steepening is a result of the different starting amplitudes for the various values of β used in the study, as seen in Figure 5.3. Once the amplitudes are normalized, the β effect is masked.

4. Figure 5.9 shows that the closed form solution found in (5.21) closely matches the series solution to the DBE in (5.9), for $\lambda \ll 1$.

5.6.2 Cole's Problem

1. Figure 5.6 shows that as λ is increased, a dampening in the amplitude of the initial sinusoidal signal is noted. Furthermore, λ mitigates the steepening effect caused by the nonlinear term, shifting the maximum amplitude back towards the midpoint.

2. Figure 5.5 shows that increasing Re (decreasing $\tilde{\nu}$) slows the decay in the signal.

3. Figure 5.5 shows how the nonlinear term, through $\tilde{\nu}$, affects the evolution of an initial sinusoidal signal. As β is increased, $\tilde{\nu}$ is decreased, which leads to a prominent steepening in the signal. This effect is also noted in Figure 5.6.

4. Figures 5.7 and 5.8 show that the approximate solution found in (5.18) holds well for the DBE for $\hat{t} \ll 1/\lambda$.

5.6.3 Relation to Other Fields

We compared our study of the DBE to related research in other fields. For the special case of $\lambda \ll 1$, the traveling wave series solution in (5.9) is found to be in agreement with the corresponding closed form solution found in the field of magnetoacoustics (5.21). We have also related our study of the DBE to a similar study in the field of relaxing media. Soluyan found an analytical solution to the inviscid DBE in the semi-infinite domain under harmonic driving, whereas we investigated the DBE in the context of the evolution of an initial sinusoidal signal on a finite domain.

CHAPTER VI

Conclusions

In this investigation, we have studied the Brinkman equation as a weakly-nonlinear model of poroacoustic propagation. In particular, we investigated the roles that the Brinkman, Darcy, and nonlinear terms play in the model. We analyzed the model under 4 special settings: The semi-infinite domain with harmonic driving, evolution on the finite domain, the nonlinear standing wave, and the traveling wave. We have found that, in general, the nonlinear term gives rise to blow-ups and shock formation. The Darcy term is a damping term which reduces the signal with increasing δ. The Brinkman term is a diffusive term, quickly dropping the amplitude of a signal with decreasing Re. Both the Darcy and Brinkman terms help to mitigate the effects of the nonlinearity, reducing the steepening effects and blow-ups. More specifically, for each setting studied, we report the following conclusions:

6.1 Harmonic Driving in a Semi-infinite Domain

1. The impact that the Brinkman viscosity term has on an acoustic signal, as can be seen in Figures 2.2 and 2.3, is found to be diffusive in nature, damping the signal faster than without its presence. With the Brinkman term being inversely proportional to the Reynolds number, high Reynolds number systems tend toward the Darcy Jordan model.

2. Because the Brinkman term is proportional to the acoustic frequency through the time

derivative of the velocity potential, the diffusive effect is masked for lower frequencies, requiring a very low Reynolds number to reveal itself. However, for higher frequency signals, physically realistic Reynolds numbers, those of the order of 5 or more, give rise to a pronounced Brinkman viscosity dependence.

3. The coefficient of nonlinearity, β, can be interpreted as the term which describes the fluid through which the acoustic signal propagates. A β value of $1 \leq \beta \leq 1.35$ corresponds to perfect gases, while $\beta \geq 2.35$ corresponds to most liquids. As can be seen in Figures 2.4 and 2.5, the dependence on the coefficient of nonlinearity β is reduced by the Brinkman viscosity term. For high frequency signals, the dependence on β is only seen with very high Reynolds number systems, those with Reynolds numbers of 5,000 or more. Smaller Reynolds numbers increase the importance of the Brinkman term, masking the effects of changing β.

4. Figure 2.6 shows that there is little to no dependence on β for low frequency signals. This is due to the cubic dependence on ω through the time derivatives of the velocity potential in the nonlinear terms.

5. As can be seen from Figures 2.4 and 2.5, while a dependence on β is realized in the full solution, the dependence is most prevalent in the 1st order correction (nonlinear) term.

6.2 Evolution of an Initial Sinusoidal Signal on a Finite Domain

1. As can be seen from Figure 3.3, the Darcy term acts as a damping term for the wave equation. A larger δ leads to faster damping of the signal.

2. The Brinkman term, like the Darcy term, acts to decay the signal. However, for low Re, this decay is diffusive in nature, decaying very quickly to zero, unlike the damped oscillatory behavior of the Darcy case, as shown by the solid curve of Figure 3.4.

3. As Re is increased, the Brinkman term decreases in strength, giving rise to a transition from a diffusive solution to a damped wave solution (Figure 3.4, dashed and dotted curves)

4. The nonlinear term gives rise to acoustical blow-ups. The time for these blow ups, as is evident in Figures 3.5(a) and 3.5(c), depends on the strength of the nonlinear term. For instance, Table 3.1 shows that for $\delta = 0.005$, smaller nonlinearities, those with $\epsilon\beta < 0.30$ show no signs of blow-ups, whereas when $\epsilon\beta > 0.40$, blow-ups occur relatively quickly, as seen in Figure 3.5(c).

5. Table 3.1 shows that the Darcy term helps mitigate blow-ups. As δ is increased, the Darcy term competes with the nonlinear term, shifting the blow-ups to later times. When the Darcy term is sufficiently large, the damping is fast enough to prevent the blow-ups from forming. For example, increasing δ from .005 to 0.05 with $\epsilon\beta = .40$ prevents the blow-up from forming, as in Figures 3.5(c) and 3.5(e).

6. The Brinkman term, when Re is small, forbids the formation of blow-ups, as can be seen in Figure 3.5. Increasing $\epsilon\beta$ shows very little effect on the evolution of the signal. However, as Re is increased, the equation transitions into a hyperbolic type equation and the damped oscillatory nature of the solution becomes dominant, allowing for blow-ups to occur. Table 3.2 shows that while in this hyperbolic regime, reducing Re shifts the blow-ups to later times, as in the Darcy case.

6.3 Nonlinear Standing Waves

1. The Brinkman model (4.4) of poroacoustic propagation permits sawtooth behavior.

2. The origin of the sawtooth behavior is the nonlinear term, as can be seen in Figure 4.2. An increase in $\epsilon\beta$ causes a more prominent steepening in the signal. This increase also gives rise to an increase in the amplification of the signal. With a very high value

of $\epsilon\beta$, the signal will eventually blow up.

3. Figure 4.3 shows that the Darcy term dampens the signal amplitude, reducing the effective steepening in the signal, and thus reducing the sawtooth behavior.

4. The Brinkman term, being a diffusive term, also lowers the signal amplitude. It can be seen from Figure 4.4 that it significantly reduces the steepening caused by the nonlinearity, forbidding the formation of the sawtooth behavior for low Re values.

5. As was found in similar equations without the Darcy and Brinkman terms, this model of poroacoustics also shows shock formation in the small time regime, as seen in Figure 4.5.

6.4 Brinkman Model Through the DBE

6.4.1 Traveling Wave

1. As shown in Figure 5.1, the drop in wave amplitude is λ dependent. An increase in λ leads to a shift in the location of the drop of the signal amplitude to shorter distances.

2. We note that an increase in Re shifts the drop of the amplitude of the signal to larger distances, as shown in Figure 5.2. Also noted in Figure 5.2, increasing Re mitigates the steepness caused by the nonlinearity.

3. The nonlinear term allows for a steepening effect. However, this steepening is a result of the different starting amplitudes for the various values of β used in the study, as seen in Figure 5.3. Once the amplitudes are normalized, the β effect is masked.

4. Figure 5.9 shows that the closed form solution found in (5.21) closely matches the series solution to the DBE in (5.9), for $\lambda \ll 1$.

6.4.2 Cole's Problem

1. Figure 5.6 shows that as λ is increased, a dampening in the amplitude of the initial sinusoidal signal is noted. Furthermore, λ mitigates the steepening effect caused by the nonlinear term, shifting the maximum amplitude back towards the midpoint.

2. Figure 5.5 shows that increasing Re (decreasing $\tilde{\nu}$) slows the decay in the signal.

3. Figure 5.5 shows how the nonlinear term, through $\tilde{\nu}$, affects the evolution of an initial sinusoidal signal. As β is increased, $\tilde{\nu}$ is decreased, which leads to a prominent steepening in the signal. This effect is also noted in Figure 5.6.

4. Figures 5.7 and 5.8 show that the approximate solution found in (5.18) holds well for the DBE for $\hat{t} \ll 1/\lambda$.

6.4.3 Relation to Other Fields

We compared our study of the DBE to related research in other fields. For the special case of $\lambda \ll 1$, the traveling wave series solution in (5.9) is found to be in agreement with the corresponding closed form solution found in the field of magnetoacoustics (5.21). We have also related our study of the DBE to a similar study in the field of relaxing media. Soluyan found an analytical solution to the inviscid damped Burgers equation in the semi-infinite domain under harmonic driving, whereas we investigated the DBE in the context of the evolution of an initial sinusoidal signal on a finite domain.

BIBLIOGRAPHY

BIBLIOGRAPHY

Beyer, R. (1997), The parameter b/a, in *Nonlinear Acoustics*, edited by M. Hamilton and D. Blackstock, pp. 25–39, Academic Press, San Diego, CA.

Burden, R., and J. Faires (1993), *Numerical Analysis*, fifth ed., PSW-Kent, Boston, MA.

Cole, J. D. (1951), On a quasi-linear parabolic equation occuring in aerodynamics, *Quarterly of Applied Mathematics*, *9*, 225–236.

Crighton, D. G. (1979), Model equations of nonlinear acoustics, *Annual Review of Fluid Mechanics*, *11*(1), 11–33, doi:10.1146/annurev.fl.11.010179.000303.

de Ville, A. (1996), On the properties of compressible gas flow in a porous media, *Transport in Porous Media*, *22*(3), 287–306.

Elmore, W., and M. Heald (1969), *Physics of Waves*, chap. 4.7, Dover Books on Physics Series, Dover Publications.

Fetter, A., and J. Walecka (1980), *Theoretical Mechanics of Particles and Continua*, pp. 413–415, Dover books on physics, Dover Publications.

Jordan, P. M. (2004), An analytical study of kuznetsov's equation: diffusive solitons, shock formation, and solution bifurcation, *Physics Letters A*, *326*(1-2), 77–84.

Jordan, P. M. (2009), Some remarks on nonlinear poroacoustic phenomena, *Mathematics and Computers in Simulation (MATCOM)*, *80*(1), 202–211.

Jordan, P. M. (2016), A survey of weakly-nonlinear acoustic models: 1910–2009, *Mech. Res. Commun.*, *73*, 127–139.

Jordan, P. M., and C. I. Christov (2005), A simple finite difference scheme for modeling the finite-time blow-up of acoustic acceleration waves, *Journal of Sound and Vibration*, *281*, 1207–1216.

Korsunskii, S. V. (1991), Propagation of nonlinear magnetoacoustic waves in electrically conductlnq dissipative media with drag, *A kusticheskii Zhurnal*, *37*, 717–722.

Malfiet, W. (1993), Approximate solution of the damped burgers equation, *Journal of Physics A: Mathematical and General*, *26*, L723–L728.

Nield, D., and A. Bejan (1999), *Convection in Porous Media: 2nd edition*, chap. 1, Springer.

Payne, L. E., J. F. Rodrigues, and B. Straughan (2001), Effect of anisotropic permeability on darcy's law, *Mathematical Methods in the Applied Sciences*, *24*(6), 427–438.

Rasmussen, A. R. (2009), Thermoviscous model equations in nonlinear acoustics, Ph.D. thesis, Technical University of Denmark.

R.E. Mickens, P. M. J. (2004), A positivity-preserving nonstandard finite difference scheme for the damped wave equation, *Numerical Methods for Partial Differential Equations*, *20*(5), 639–649.

Rossmanith, D. A., and A. Puri (2014), The role of brinkman viscosity in poroacoustic propagation, *International Journal of Non-Linear Mechanics*, *67*, 1–6.

Rossmanith, D. A., and A. Puri (2016), Non-linear evolution of a sinusoidal pulse under a brinkman-based poroacoustic model, *International Journal of Non-Linear Mechanics*, *78*, 53–58.

Soluyan, S. I., and R. V. Khokhlov (1962), Finite amplitude acoustic waves in a relaxing medium, *A kusticheskii Zhurnal*, *8*, 220–227.

Straughan, B. (2008), *Stability and Wave Motion in Porous Media*, Applied Mathematical Sciences, Springer.

Thompson, P. (1972), *Compressible-fluid dynamics*, Advanced engineering series, McGraw-Hill.

Wei, D., and P. M. Jordan (2013), A note on acoustic propagation in power-law fluids: Compact kinks, mild discontinuities, and a connection to finite-scale theory, *International Journal of Non-Linear Mechanics*, *48*(1), 72–77.

Wells, P. N. T. (1999), Ultrasonic imaging of the human body, *Reports on Progress in Physics*, *62*(5), 671.

List of Publications

1. Rossmanith, D. A., and A. Puri (2014), The role of brinkman viscosity in poroacoustic propagation, International Journal of Non-Linear Mechanics, 67, 1–6.

2. Rossmanith, D. A., and A. Puri (2016), Non-linear evolution of a sinusoidal pulse under a brinkman-based poroacoustic model, International Journal of Non-Linear Mechanics, 78, 53–58.

3. Rossmanith, D. A., and A. Puri (To be submitted), A recasting of Brinkman's equation as Burgers equation, Evolution Equations and Control Theory.

VITA

The author was born in Metairie, Louisiana in April of 1982. He received a B.S. in Physics at the University of New Orleans in 2008. He went on to earn a M.S. in Applied Physics at the University of New Orleans in 2014. During this pursuit, he was given the opportunity to work on a research project in the field of poroacoustics. Through this research project, David published multiple articles on the subject and has given a lecture at the International Association for Mathematics and Computer Simulation (IMACS) conference in 2013.